



## Ice Core Science at the three Poles



# Annual Report 2022

Laboratory of Environmental Chemistry

**On the cover page:**

From 2 to 7 October 2022, the international ice core science community assembled for its third Open Science Conference (OSC) in Crans-Montana, Switzerland. The OSC brought together 270 ice core scientists from 20 countries working on the Greenland and Antarctic Ice Sheet as well as high-altitude glaciers; hence the theme of the conference was chosen to be “Ice core sciences at the three poles”.

Please see report on page 28.

PAUL SCHERRER INSTITUT



# Annual Report 2022

Laboratory of Environmental Chemistry

**Editors**

M. Schwikowski, M. Ammann

**Paul Scherrer Institut**

Laboratory of Environmental Chemistry

Forschungsstrasse 111

5232 Villigen PSI

Switzerland

Phone +41 56 310 25 05

[www.psi.ch/luc](http://www.psi.ch/luc)

Reports are available: [www.psi.ch/luc/annual-reports](http://www.psi.ch/luc/annual-reports)





## TABLE OF CONTENT

Editorial.....	1
Surface Chemistry	
THE UNDESIRABLES OF SYNTHETIC FUEL PRODUCTION P. A. Alpert, M. Ammann, L. Torrent, C. Ludwig, F. Vogel, H. Xiang, D. Baudouin.....	3
SOOT AND OIL NANOPARTICLE EMISSIONS FROM AIRCRAFT ENGINES P. A. Alpert, K. Kilchhofer, F. Mahrt, M. Ammann, B. Testa, Z. A. Kanji, Z. Decker, B. Brem.....	4
NOT ALL TYPES OF SECONDARY ORGANIC AEROSOL MIX F. Mahrt, L. Peng, J. Zaks, Y. Huang, P. E. Ohno, N. R. Smith, F. K.A. Gregson, Y.M. Qin, C. L. Faiola, Scot T. Martin, S. A. Nizkorodov, M. Ammann, A. K. Bertram.....	5
THE IRON AGE(ING) OF SECONDARY ORGANIC AEROSOL N. M. Garner, J. Top, F. Mahrt, I. El Haddad, M. Ammann, D. M. Bell.....	6
ENHANCED OXIDATIVE POTENTIAL OF PHOTOCHEMICALLY AGED AEROSOLS K. Kilchhofer, A. Barth, B. Utinger, M. Kalberer, M. Ammann.....	7
MODELING PHOTOCHEMISTRY IN IRON-CONTAINING ORGANIC AEROSOL K. Kilchhofer, A. Mishra, T. Berkemeier, P. A. Alpert, M. Ammann.....	8
CONVERSION OF NO <sub>2</sub> INDUCED BY IRON(III) CARBOXYLATE PHOTOLYSIS L. Iezzi, K. Kilchhofer, Y. Manoharan, P. A. Alpert, T. Bartels-Rausch, M. Ammann.....	9
IODINE SPECIATION RESULTING FROM IRON ORGANIC COMPLEX PHOTOLYSIS L. Iezzi, M. Reza, H. Finkenzeller, R. L. Mauldin, A. Roose, T. Bartels-Rausch, R. Volkamer, M. Ammann.....	10
THE SURFACE PROPENSITY OF IODINE SPECIES FROM THEORY A. Roose, M. Ammann, M. Krack.....	11
THE SURFACE PROPENSITY OF IODINE SPECIES FROM LIQUID JET XPS A. Roose, A. Boucly, H. Yang, L. Iezzi, M. Ammann, L. Artiglia.....	12
ICE AND CLAY: AN HYDROGEN BONDING INTERPLAY L. Longetti, Y. Manoharan, L. Artiglia, D. Pergolesi, T. Bartels-Rausch.....	13
THE COLD FINGER Y. Manoharan, A. Laso, M. Ammann, T. Bartels-Rausch.....	14
NITRIC ACID DISSOCIATION AT THE AIR-ICE INTERFACE Y. Manoharan, L. Longetti, M. Ammann, T. Bartels-Rausch.....	15
ACID-BASE CHEMISTRY OF AMMONIA AT THE ICE-VAPOR INTERFACE C. Richter, S. Gholami, Y. Manoharan, T. Buttersack, L. Longetti, L. Artiglia, M. Ammann, T. Bartels-Rausch, H. Blum.....	16
MODELLING CHEMISTRY IN SNOW T. Bartels-Rausch, J. Thomas, J. Stutz.....	17

## Analytical Chemistry

RECENT DECREASE IN HEAVY METAL POLLUTION FROM THE FSU REGION A. Eichler, P. Nalivaika, T. M. Jenk, T. Singer, S. Kakareka, T. Kukharchyk, S. Eyrikh, T. Papina, M. Schwikowski.....	18
ANALYSIS OF TRACE ELEMENTS IN GLACIER ICE WITH ICP-TOF-MS T. S. Münster, T. M. Jenk, A. Eichler, G. Lee, M. Schwikowski.....	19
PRE-INDUSTRIAL TO INDUSTRIAL CHANGES OF ORGANIC AEROSOLS T. Singer, T. M. Jenk, F. Burgay, J. Strähl, S. Szidat, M. Schwikowski.....	20
FIRST GLANCE AT RECENT ORGANIC RECORD ON GRAND COMBIN C. J. Huber, F. Burgay, A. Eichler, T. M. Jenk, D. Salionov, S. Bjelić, M. Schwikowski.....	21
INSIGHTS FROM THE NON-TARGET ANALYSIS OF THE BELUKHA ICE CORE F. Burgay, D. Salionov, S. Bjelic, C. J. Huber, A. Eichler, T. Singer, M. Schwikowski.....	22
BOREHOLE HORIZONTAL DISPLACEMENT AS A TOOL FOR ICE CORE DATING? T. M. Jenk, P. Gabrielli.....	23
PRELIMINARY RESULTS FROM THE ADAMELLO TEMPERATE ICE CORE G. Baccolo, S. Brüttsch, S. O. Brugger, M. Schwikowski, P. Bohleber.....	24
RADIOCARBON DATING OF A SVALBARD HORIZONTAL ICE CORE W. F. Hartz, T. M. Jenk, T. Singer, M. Schwikowski, A. Hodson.....	25
RECENT AIR POLLUTION DECREASE IN THE EURASIAN ARCTIC R. Kron, A. Eichler, S. Brüttsch, T. S. Münster, T. Tessorndorf, T. Opel, H. Meyer, M. Schwikowski.....	26
ICE CORE ACTIVITIES IN THE PAMIR PROJECT M. Schwikowski, T. M. Jenk, F. Burgay, C. Mayer, A. Lambrecht, E. Miles.....	27
ICE CORE SCIENCES AT THE THREE POLES M. Schwikowski, H. Fischer.....	28
List of Publications.....	29
Affiliation Index.....	31

**EDITORIAL**

The year 2022 was a turbulent and challenging one for our Laboratory of Environmental Chemistry (LUC). With the lift of COVID-related measures, life returned to labs, offices and coffee-rooms and also the advantages of attending conferences, workshops and meetings in person were rediscovered.

Not only attending, but also organizing conferences was possible again. In October 2022 the international ice core science community assembled, after postponing twice, for its third open science conference in Crans-Montana with the theme "Ice Core Science at the three Poles." This remarkable event was co-organized by members of the Analytical Chemistry Group and the Climate Physics of the University of Bern, see report on page 28 and cover page. In December 2022 the 9<sup>th</sup> international workshop on ambient pressure X-ray photoelectron spectroscopy was hosted by the Paul Scherrer Institute at the University of Applied Sciences in Windisch, organized by members of the Surface Chemistry Group. For both events the perfect organization by conference manager Doris Bühler was key for the success.

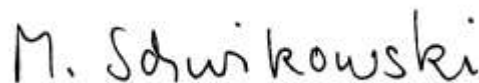
Silvia Köchli, our chemical lab technician, retired last year after working for 19 years in the Analytical Chemistry Group. She was responsible for service analyses of various major and trace elements in a broad range of materials and samples for customers from entire PSI. Many thanks and enjoy your well-deserved retirement, Silvia.

Two students of the Surface Chemistry Group successfully defended their PhD at the ETH Zürich: On 7th April 2022 Shuzhen Chen with her thesis entitled "Mul-

tiphase kinetics and chemistry at halide solution-air interfaces" and on 26th September 2022 Jérôme Gabathuler with his thesis entitled "The thickness of the quasi-liquid layer on ice and its interaction with atmospheric gases as seen by X-ray absorption and photoelectron spectroscopies". Congratulations to both of them!

In November 2022 we were informed by PSI that the ice core research conducted by the Analytical Chemistry Group will not continue at PSI after my retirement at the end of November 2024 and at the same time the Laboratory of Environmental Chemistry will be dissolved. As a first consequence, the Surface Chemistry Group was merged with the Laboratory of Atmospheric Chemistry (LAC) as of February 2023, when the new LAC lab head Claudia Mohr started.

Hence, this will be the last Annual Report, which we publish as Laboratory of Environmental Chemistry. With that a long tradition will come to an end, which started with the first edition of the Laboratory of Radiochemistry and Environmental Chemistry (LCH) in 1988, and continued from 2016 with two separate reports, one from Laboratory of Radiochemistry and the other from the Laboratory of Environmental Chemistry. I wish you nevertheless an enjoyable reading and thank you for your interest in our research.



Margit Schwikowski



## THE UNDESIRABLES OF SYNTHETIC FUEL PRODUCTION

*P. A. Alpert, M. Ammann (PSI LUC), L. Torrent, C. Ludwig, F. Vogel, H. Xiang, D. Baudouin (PSI LBK)*

**Reducing the amount of undesired products during synthetic fuel production is very important. To that end, we characterized the composition of particulate and soluble byproducts after the synthetic production of biocrude from hydrothermal processing.**

Hydrothermal gasification (HTG) and liquefaction (HTL) are technologies used to convert various biogenic feedstocks, such as microbial cultures, sewer sludge, black liquor and waste wood sawdust into sustainable gaseous and liquid fuels, respectively. These processes, which operate in or near supercritical water, rely on catalysts for selective fuel or gas production and heavily rely on the selective removal of unwanted carbonaceous particles or non-carbonaceous salts and compounds [1]. The efficient recovery of brine (water and salts) is very important to protect any scavenger or catalyst that is used downstream, and relevant for recuperating costs by producing fertilizer [2]. On the other end, understanding the formation and the fate of carbonaceous particles during such processes is of great importance to understand the impact of conditions, e.g. temperature, pressure, and time on the biocrude or the biogas production yield and composition. Indeed, the formation of carbonaceous deposits on the catalyst grains (macroscopic scale) and active sites (nanoscopic scale) is an important cause of deactivation, preventing long term operation and reducing biofuels/biogas yields and selectivity.

Here, we report on our efforts to investigate particles and soluble compounds generated from HTL of spruce wood using scanning transmission X-ray microscopy coupled to near-edge X-ray absorption fine structure spectroscopy (STXM/NEXAFS). With this purpose, the HTL reaction was carried out in a batch reactor setup [3] applying spruce wood sawdust as the feedstock at 350 °C, 17 MPa and 20 min. The desired product of this HTL experiment was the biocrude, which has great potential to be refined into liquid fuel. The undesired solid particles and aqueous phase compounds were also investigated.

Fig. 1 shows that the compounds generated during HTL are fairly different in terms of peak height, but have nearly identical peak position in terms of energy. For example, matter found in the aqueous phase (blue line) has the largest peak height at about 288.6 eV indicating organic carboxylic acids and another contribution from sp<sup>2</sup> hybridization at 285.4 eV and potentially phenolic compounds at 287.1 eV. The desired biocrude oil (red line) has relatively little carboxyl contribution, but also has the same peaks as the aqueous phase carbonaceous matter. This implies that carboxylic substitutions on these compounds may cause them to be more water soluble.

We can conclude from these results that dominant functionalities that make up the desired and undesired by-products of HTL are quite similar overall. This implies that the difference we do see could be used to target specific processes to convert, e.g. aqueous phase compounds to biocrude through decarboxylation steps to remove oxygen. This would also benefit the production of aircraft fuels in next steps of fuel production since this fuel type requires nearly zero oxygen content.

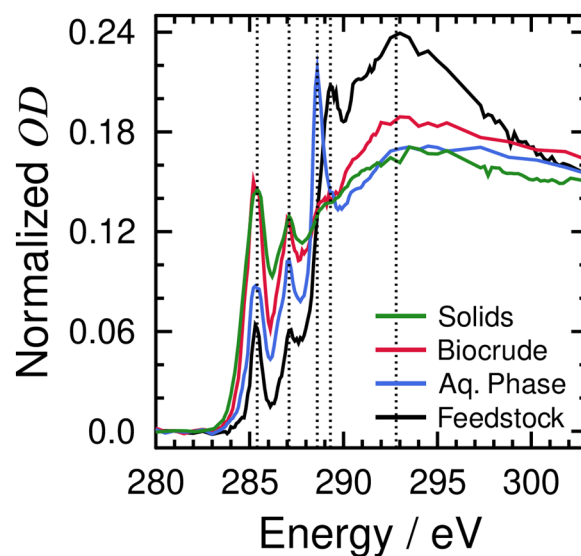


**Fig. 1:** Carbon NEXAFS spectra of various compounds and particles found during HTL. The vertical dashed lines indicate the peaks at 285.4 eV, 287.1 eV, 288.6 eV, 289.3 eV and 292.8 eV. The feedstock was spruce wood sawdust prior to HTL and solid particles, aqueous solution and biocrude oil were formed after HTL. Spectra were pre-edge subtracted (278.0 – 302.0 eV) and normalized to the total carbon, which is the spectral area between 310.0 and 320.0 eV.

We acknowledge funding from the SynFuel joint initiative, Competence Center for Product Stream Analytics, Grant 320022.

- [1] M. Schubert et al., *The Journal of Supercritical Fluids*, **61**, 44-54 (2012).
- [2] J. Reimer et al., *The Journal of Supercritical Fluids*, **117**, 113-121 (2016).
- [3] M. H. Waldner et al., *Industrial & Engineering Chemistry Research*, **44**, 4543-4551 (2005).

## SOOT AND OIL NANOPARTICLE EMISSIONS FROM AIRCRAFT ENGINES

*P. A. Alpert (PSI LUC), K. Kilchhofer (PSI LUC, ETHZ), F. Mahrt (PSI LUC), M. Ammann (PSI LUC), B. Testa, Z. A. Kanji (ETHZ), Z. Decker, B. Brem (PSI LAC)*

**Harmful gasses and aerosol particles are a health risk when inhaled. We quantify the concentration and composition of commercial aircraft engine emissions and identify their contribution to ambient air nearby Zurich airport and to ice cloud formation.**

Combustion in aircraft engines generate particulate matter (PM), which can induce oxidative stress in bronchial cells, as well as pulmonary and respiratory inflammation. This is especially the case for emission during idling and taxiing engine operation [1]. At the engine exit plane, soot is the main particulate pollutant, like at any other combustion engine. However, lubrication oil is hypothesized here to be a significant fraction of emissions [2], and contains additives, such as tricresyl phosphates, and metals linked to neurotoxicity [3, 4]. Our aim is to characterize particulate emissions directly from aircraft engines by chemically distinguishing between single or mixed soot and oil particles.

Single particle analysis was performed using scanning transmission X-ray microscopy coupled with near-edge X-ray absorption fine structure spectroscopy (STXM/NEXAFS). Here, X-rays were used to resolve chemical detail on a scale of tens of nanometers. In collaboration with the Zurich University of Applied Sciences (ZHAW) Centre for Aviation, we sampled particles from in-service turbofans in the silencer of the engine Test Cell at SR Technics. Engines after previous repair and overhaul are tested for their performance in the Test Cell. The silencer part of the Test Cell is a large building designed to muffle sound and safely direct emissions away from the staff and surrounding work area. Particles sampled from the silencer were directed to either a multi-orifice uniform deposition impactor (MOUDI) or an electrostatic precipitator onto suitable substrates for further analysis.

Fig. 1 shows two X-ray optical density, OD, images of particles emitted from an aircraft engine and their characteristic NEXAFS. At an X-ray energy of A) 285.4 eV, particles of soot are clearly seen. We found an absorption peak at B) 287.5 eV indicating oxygenated carbon functions that are more organic-like. This peak is highly characteristic of aircraft soot and independent on whether a catalytic stripper was used to remove volatile matter. This unique composition also seen in the absorption spectra in Fig. 1C indicates quinone functionalities and non-soot like aliphatic carbon [5]. Preliminary atomic resolution transmission electron microscopy results yield an amorphous coating on the soot similar to that found in our previous research [6]. However, this composition is not typical of soot from other combustion and urban sources [7] shown as grey lines in Fig. 1C, that typically have a spectral signature of carboxyl functionalities (COOH). We hypothesize that

atmospheric processing and oxidation will generate carboxyl functions, and that fresh aircraft soot will be identified in the vicinity of the airport using this unique chemical marker at 287.5 eV during our upcoming field campaign.

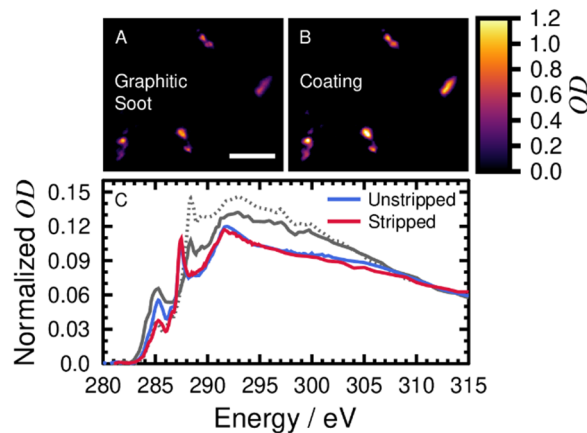


**Fig. 1:** Optical density,  $OD$ , images and NEXAFS of soot emitted from a Pratt & Whitney 4000-94” engine. Images were acquired at an X-ray energy of A) 285.4 eV indicating contributions from graphitic soot and B) 287.6 eV indicated contributions of oxygenated coatings. The scale bar is 2  $\mu\text{m}$  and applies to both images. C) Normalized NEXAFS of particles when a catalytic stripper was operated or not indicated in the legend as “Stripped” and “Unstripped”, respectively. Reference spectra of soot from urban sources are shown that are heavily impacted by organics (solid grey line) or not (dotted grey line) [7].

We acknowledge funding from the Swiss Federal Office of Civil Aviation (SFLV 2020-080).

- [1] H. R. Jonsdottir et al., *Communications Biology*, **2**, 90 (2019).
- [2] Z. Yu et al., *Environ. Sci. Technol.*, **46**, 9630-9637 (2012).
- [3] D. Johnson et al., *Journal of Mass Spectrometry*, **50**, 683-692 (2015).
- [4] M. F. Rahim et al., *Environ. Pollut.*, **246**, 734-744 (2019).
- [5] R. J. Hopkins et al., *J. Aerosol Sci.*, **38**, 573-591 (2007).
- [6] A. Liati et al., *Environ. Pollut.*, **247**, 658-667 (2019).
- [7] R. C. Moffet et al., *Anal. Chem.*, **82**, 7906-7914 (2010).

## NOT ALL TYPES OF SECONDARY ORGANIC AEROSOL MIX

F. Mahrt (PSI LUC, UBC), L. Peng, J. Zaks (UBC), Y. Huang (UBC), P. E. Ohno (HU), N. R. Smith (UCI), F. K. A. Gregson (UBC), Y. M. Qin (HU), C. L. Faiola (UCI), S. T. Martin (HU), S. A. Nizkorodov (UCI), M. Ammann (PSI LUC), A. K. Bertram (UBC)

**Secondary organic aerosol (SOA) constitutes a large fraction of ambient aerosol. Here, we investigate the number of phases in particles that are mixtures of different SOA types. We identify drivers for the number of phases formed.**

A large mass fraction of atmospheric aerosols is composed of secondary organic aerosol (SOA), which is important for air pollution and climate. SOA is mainly formed through oxidation of volatile organic compounds (VOC) from both anthropogenic and biogenic sources, followed by gas-particle partitioning of the reaction products [1]. Given the large variety of VOCs and oxidation pathways many different SOA types exist in the atmosphere. The elemental oxygen-to-carbon (O/C) ratio can be used to classify SOA into semi-volatile oxygenated organic aerosol (SV-OOA) with O/C ratios roughly between 0.32 and 0.83, and low-volatility oxygenated organic aerosol (LV-OOA) with O/C ratios roughly between 0.68 and 1.32 [2]. SV-OOA represents fresh, less oxidized SOA, whereas LV-OOA represents aged, more oxidized SOA. During atmospheric transport different SOA types often become internally mixed forming SOA+SOA particles. Information on the number of phases, in such SOA+SOA particles is important to predict the role of SOA for air pollution and climate. This is because the number of phases impacts many processes including heterogeneous chemical reactions, gas-particle partitioning and in turn particle growth and size distribution, ultimately affecting climate. Atmospheric models often assume that different SOA types form a single phase when internally mixed. If different SOA types are completely miscible the presence of SOA seed particles enhances SOA formation, by providing additional condensed mass for VOCs to partition into. Such enhancement is absent, if SOA+SOA mixtures form two distinct condensed phases. Here, we investigated the number of phases formed in mixtures of two different SOA types that were generated in environmental chambers from oxidation of different VOCs. The number of phases directly observed as a function of relative humidity (RH), using fluorescence microscopy, and SOA types were characterized using an aerosol mass spectrometer.

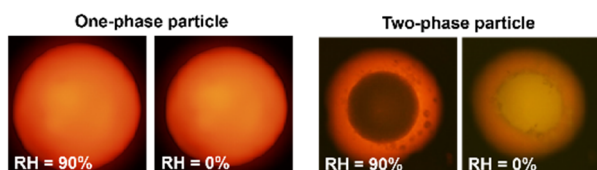


**Fig. 1:** Images of one and two-phase SOA+SOA particles at different RH. Right:  $\beta$ -caryophyllene/ $O_3$  SOA +  $\alpha$ -pinene/ $O_3$  SOA. Left:  $\beta$ -caryophyllene/ $O_3$  SOA + toluene/ $OH$  SOA.

Fig. 1 shows example microscopy images, for SOA+SOA mixtures, revealing that particles with either one or two phases can form, depending on the O/C of the components and the RH. For all our SOA+SOA mixtures the number of phases was found to be independent of humidity between 90 to 0 % RH.

Fig. 2 summarizes the number of non-crystalline phases observed in our experiments, for all SOA+SOA mixtures investigated. Our results reveal a strong dependence of the number of phases on the difference in average O/C ratio between the two SOA types mixed,  $\Delta(O/C)$ . Specifically, we found one- and two-phase particles for  $\Delta(O/C) < 0.47$  and  $\Delta(O/C) \geq 0.47$ .

Overall, our results suggest that not all SOA types mix, challenging the assumption often made in modelling studies. In particular, our results suggest that while fresh and aged SOA can form two-phase particles if their  $\Delta(O/C) \geq 0.47$ , this can change during atmospheric aging, when different SOA types become oxidized and their O/C ratios become more similar.

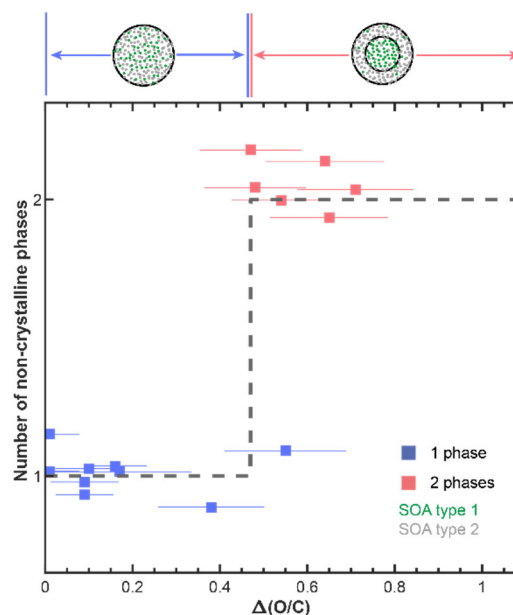


**Fig. 2:** Number of phases observed for SOA+SOA mixtures as a function of their  $\Delta(O/C)$  and 90-0% RH.

We acknowledge funding from European Union's Horizon 2020 research and innovation programme under the Marie Skłodowska-Curie grant agreement no. 890200.

- [1] J. L. Jimenez et al., *Science*, **326**, 1525 (2009).
- [2] M. R. Canagaratna et al., *Atmos. Chem. Phys.*, **15** 253-272 (2015).
- [3] F. Mahrt et al., *Atmos. Chem. Phys.*, **22** 13783-13796 (2022).

## THE IRON AGE(ING) OF SECONDARY ORGANIC AEROSOL

N. M. Garner (PSI LUC), J. Top (PSI LAC, ETHZ), F. Mahrt (PSI LUC), I. El Haddad (PSI LAC),  
M. Ammann (PSI LUC), D. M. Bell (PSI LAC)

**Secondary organic aerosol (SOA) can undergo physical and chemical aging processes that alter their impact on climate, air quality and human health. One way this can occur is via reactions of transition metals, such as iron, with condensed-phase organics.**

Iron-containing particles (from mineral dust, and particles emitted from combustion and industrial processes), can often become internally mixed with SOA [1]. When organic vapors condense on metal containing particles, they can facilitate dissolution of minerals and form iron-organic complexes [1]. Iron-organic complexes are common in atmospheric particles [2] and can generate reactive oxygen species within a particle through dark peroxide and photochemical reactions (i.e., Fenton chemistry), leading to further functionalization or fragmentation of organic species [1,3]. These processes depend on the chemical structure and functional groups of the aerosol components, which are often chemically complex, comprising of numerous organic compounds. As such, particle phase aging processes are intricate and detailed understanding of these is lacking to date; hence, considerable uncertainties remain regarding the impact aged particles have on air quality and climate.

Here, we present data on the chemical composition of iron-containing SOA particles. Particles were produced by forming SOA via  $\alpha$ -pinene (aP,  $C_{10}H_{16}$ ) ozonolysis on both ammonium sulfate (AS) or iron-containing seed particles in an atmospheric simulation chamber under dark conditions. This allowed us to probe the impact of dark e.g., peroxide reactions on aerosol aging in the absence of photochemically driven Fenton chemistry, i.e., simulating nocturnal aging processes. Using an extractive electro-spray ionization mass spectrometer, high time resolution molecular-level data on condensed-phase oxidation products present within the particles, i.e., monomers and dimers, were obtained. Aerosol mass was monitored using a scanning mobility particle sizer.

Sample time series of SOA generated using AS and iron-containing seed particles are shown in Figure 1 as the dark blue and black traces respectively.  $\sim 70 \mu\text{g m}^{-3}$  seed particles were added to the chamber before aP was injected (at 00:30). After  $\sim 1$  hr (01:30), the rate of SOA mass production slowed, and is denoted as T1. Figure 2 shows example bar graphs of monomers and dimers present in aerosol at T1. Monomers are degradation products of aP oxidation, and dimers result from their subsequent reaction. Although major species such as  $C_9H_{14}O_x$  and  $C_{10}H_{16}O_x$  were present in both aerosol types, the ratios between these species, as well as overall monomer/dimer ratios varied in the presence/absence of iron. This suggests that transition metals can affect the aging of SOA; however, the mechanisms through which this occurs remain under investigation.

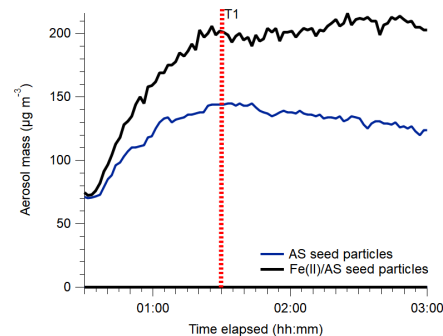


**Fig. 1:** Time series of SOA generated during the experiments, and where aP was injected into the chamber at 00:30. The offset in aerosol mass is the initial mass (in  $\mu\text{g m}^{-3}$ ) of seed particles in the chamber. The composition of aerosol, labeled T1 (red dashed line), is shown below in Fig. 2.

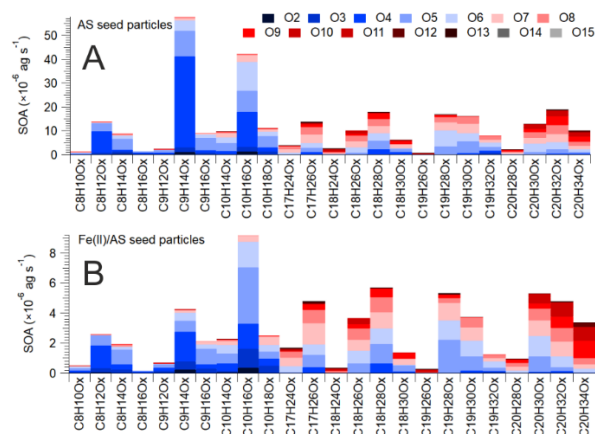


**Fig. 2:** Bar graphs of monomers and dimers present in aerosol, 1 hr after the addition of aP to the chamber (T1, Figure 1). SOA species are shown as a mass flux ( $\text{ag s}^{-1}$ ). Panel A shows an example experiment where aerosol were generated on ammonium sulfate seed particles, and panel B shows an experiment on iron-containing seed particles. Both experiments were conducted at a relative humidity  $>80\%$ .

We acknowledge funding from the Swiss National Science Foundation (Grant 188662).

- [1] L. Deguillaume et al., *Chem. Rev.*, **105** (9), 3388-3431 (2005).
- [2] A. Tapparo et al., *Chemosphere*, **241**, 125025 (2020).
- [3] K. E. Daumit et al., *J. Phys. Chem. A*, **120**, 1386-1394 (2016).

## ENHANCED OXIDATIVE POTENTIAL OF PHOTOCHEMICALLY AGED AEROSOLS

K. Kilchhofer (PSI LUC, ETHZ), A. Barth, B. Uttinger, M. Kalberer (Univ. Basel), M. Ammann (PSI LUC)

**Photolysis of iron-carboxylate complexes in viscous organic aerosol (OA) can produce harmful reactive oxygen species (ROS). With online aerosol flow tube experiments, we confirm enhanced ROS production in iron containing OAs exposed to UV-light.**

Reactive oxygen species (ROS) affect human health via inducing oxidative stress upon inhalation [1]. Recent work in our group showed that processes initiated by iron-citrate complex photolysis in organic aerosol (OA) leads to the formation of carbon centered free radicals (i.e. ROS) [2]. This, in combination with low diffusivity due to high viscosity of OA at low relative humidity, leads to anoxic conditions in the interior of the particles [2]. ROS may only be released when higher relative humidity (RH) is reached (in the lung). In this project, we examine ROS concentrations in photochemically aged iron-citrate aerosol particles.

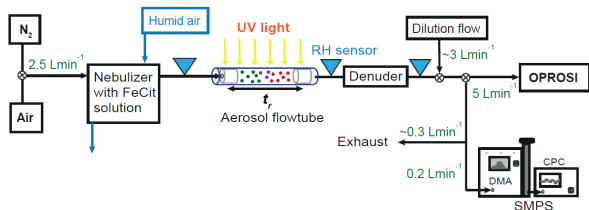


**Fig. 1:** Schematic of the aerosol flow tube setup. The residence time ( $t_r$ ) in the aerosol flow tube including seven UV lamps was set to 3 min. The denuder removes all the gas phase species from the product gas flow (green). The SMPS measures the aerosol number concentration and size distribution.

ROS is measured by an online particle-bound ROS instrument (OPROSI, [3]) connected to a newly developed aerosol flow tube (AFT) setup as shown in Fig. 1. The SMPS system is used to monitor the aerosol number concentration and size distribution during an experiment. The model aerosol (iron-citrate/citric acid mixture) is nebulized into the system with either air or nitrogen as carrier gas. A humidifier controls the RH. A denuder downstream of the AFT takes up all the volatile species in the gas flow, which might interfere with the ROS quantification by the OPROSI. The novelty of this system is that it is able to measure ROS directly in the aerosol particles (particle-bound ROS) and directly after being photochemically aged in the aerosol flow tube (online). OPROSI allows us to measure continuously using a chemical assay of 2'7'-dichlorofluorescein (DCFH) with a horseradish peroxidase (HRP), via fluorescence spectroscopy. It shows a fast response to changes in concentrations of laboratory-generated oxidized OA [3], directly relevant for this work.

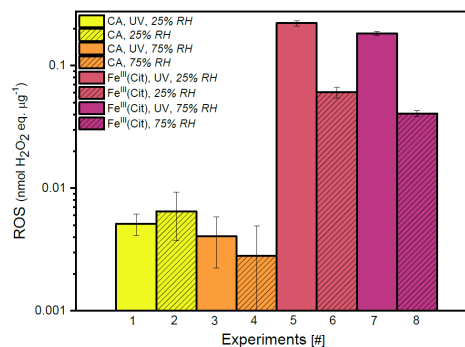


**Fig. 2:** ROS concentrations produced at different relative humidity conditions ( $RH = 25$  or  $75\%$ ). The color denotes the RH. The plain bars represent the ROS signal under UV irradiation, while the hashed bars denote the corresponding dark conditions.

The ROS concentrations (nmol H<sub>2</sub>O<sub>2</sub> equivalents per mass of particle) from eight flow tube experiments are plotted in Fig. 2. The hashed bars represent dark measurement periods, whereas the plain bars denote the UV irradiation periods. Pure citric acid (CA) experiments were conducted for detecting the background ROS concentration (yellow and orange bars). Each experiment was carried out at high ( $75\%$ ) and low ( $25\%$ ) RH. The results show a remarkably higher ROS concentration in the case of iron-citrate aerosols (dark and UV exposed) compared to experiments with CA only. Also, the ROS concentrations of the iron-citrate samples are significantly enhanced while being UV exposed and ROS production tends to be higher at dryer conditions ( $RH = 25\%$ ).

In a second campaign, some of the experiments will be repeated and copper will be added in order to quantify a possible change in the ROS production upon photochemical OA aging. This will help understanding an iron-copper catalytic cycle and the behavior of iron-carboxylate photochemistry coupled to an additional transition metal.

We acknowledge funding from the Swiss National Science Foundation (Grant 188662).

- [1] N. L. Ng et al., Health Effects Institute, 197, (2019).
- [2] P. A. Alpert et al., Nature Comm., **12**, 1769, (2021).
- [3] F. P. H. Wragg et al., Atmos. Meas. Tech., **9**, 4891-4900 (2016).

# MODELING PHOTOCHEMISTRY IN IRON-CONTAINING ORGANIC AEROSOL

K. Kilchhofer (PSI LUC, ETHZ), A. Mishra, T. Berkemeier (MPIC), P. A. Alpert, M. Ammann (PSI LUC)

**We simulate the dissociation of iron-carboxylate complexes and secondary chemistry in viscous organic aerosols with a new kinetic multi-layer model. We model CO<sub>2</sub> production and release to the gas phase of coated wall flowtube experiments.**

Transition metal ions (TMI) such as iron play an important role in the atmosphere's photochemical aging process of organic aerosols (OA) [1]. TMI complexes result in building-up of harmful species in the interior of the particles [2].

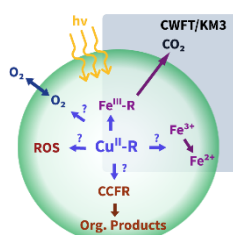


**Fig. 1:** Schematic of iron-copper-citrate aerosol with used experimental/computational methods (grey box). The question marks are referring to the open research questions regarding the impact of copper in the existing iron-citrate system. CCFR: carbon-centered free radical

Fig. 1 depicts the model aerosol (iron-copper-citrate-citric acid) used in this study including the schematically drawn chemical mechanisms and physical properties/diffusion paths of, e.g., oxygen (O<sub>2</sub>) in blue and CO<sub>2</sub> in black. The grey box depicts the species (CO<sub>2</sub>) examined here. The overarching goal of this project is to assess the influence of copper (see question marks in Fig. 1) in the iron-citrate aerosol system, building on our previous studies toward understanding the build-up of reactive oxygen species (ROS) in dependence of the OA's viscosity [2]. For this purpose, we first conducted coated wall flow tube (CWFT) experiments to measure CO<sub>2</sub> emitted into the gas phase following decarboxylation after photolysis of an iron-citrate complex (Fe<sup>III</sup>-R). Experiments at varying humidity, iron-to-citric acid mole ratio, and light exposure time (mimicked by ultraviolet (UV) lamps) were performed in order to cover a wide range of atmospherically relevant conditions. These data are then used to validate the kinetic modeling approach.

A newly adapted kinetic multi-layer model (KM<sup>3</sup>) based on KM-SUB [3] is used to model iron-citrate photochemistry in aerosol particles. We implemented a chemical mechanism similar to the one described by Dou et al. [4] and applied the same physical parameters as used there or provided by references therein. However, the complicated equilibria of the metal complexes and the pH equilibria are re-calculated with a new algorithm developed for this iron-citrate system.

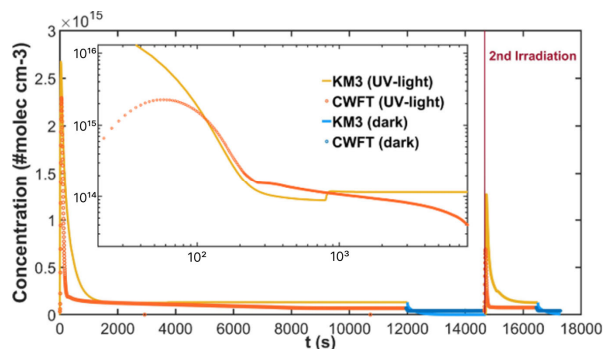


**Fig. 2:** Time series of the CO<sub>2</sub> mixing ratio produced by photolysis of the iron-citrate complex modeled (yellow-line) and measured (orange circles). The first irradiation period is represented in the inset on log log scales.

Fig. 2 shows the model (KM<sup>3</sup>) and experimental output (CWFT) of the CO<sub>2</sub> release during two irradiation exposures of the iron-citrate sample (mole ratio FeCit:CA = 1:10) at a relative humidity equal to 65 %. The initial, sharp peak represents the CO<sub>2</sub> concentration in the gas phase resulting from photolysis of the initially available iron citrate. It reaches a concentration of around  $2.5 \times 10^{15}$  molecules cm<sup>-3</sup>, and is modeled by KM<sup>3</sup> to  $2.3 \times 10^{15}$  molecules cm<sup>-3</sup>. Moreover, we are able to model the steady-state CO<sub>2</sub> production during UV irradiation, reproduce the dark mode concentration, and another CO<sub>2</sub> peak upon photolysis on the same film in a second irradiation step. The slower concentration decrease in the model during the steady state periods might be due to uncertainties in the bulk diffusion coefficients or in the chemical mechanism lacking decarboxylation pathways of products. Further model optimizations are needed to confirm this.

Additionally, we intend to measure iron-copper-citrate particles in CWFT experiments and, in parallel, model the new system with a hypothesized iron-copper catalytic cycle in KM<sup>3</sup>. This will help to understand the impact of transition metals on OA degradation and ROS production in the atmosphere at different phase states.

We acknowledge funding from the Swiss National Science Foundation (Grant 188662).

- [1] H. A. Al-Abadleh, *Environ. Sci.: Atmos.*, **1**, 297-345 (2021).
- [2] P. A. Alpert et al., *Nature Comm.*, **12**, 1769 (2021).
- [3] M. Shiraiwa et al., *Atmos. Chem. Phys.*, **10**, 3673-3691 (2010).
- [4] J. Dou et al., *Atmos. Chem. Phys.*, **21**, 315-338 (2021).

## CONVERSION OF NO<sub>2</sub> INDUCED BY IRON(III) CARBOXYLATE PHOTOLYSIS

*L. Iezzi, K. Kilchhofer, Y. Manoharan (PSI LUC, ETHZ), P. A. Alpert, T. Bartels-Rausch (PSI LUC), M. Ammann (PSI LUC)*

**Iron(III) carboxylate photochemistry can generate Reactive Oxygen Species (ROS). Here, we investigate the role of ROS for the conversion of NO<sub>2</sub> into HONO in secondary organic aerosol proxies with coated wall flow tube experiments (CWFT).**

Nitrous acid (HONO) plays a central role in atmospheric chemistry as a direct source of hydroxyl radicals (OH), which is the most important oxidizing species in the troposphere. Nevertheless, to date the formation mechanism of HONO during daytime is still not completely understood. Since direct emission, homogeneous gas-phase and heterogeneous reactions are not able to explain the observed daytime HONO concentrations, the scientific efforts have been focused on photoenhanced processes involving nitrogen dioxide (NO<sub>2</sub>) [1]. Furthermore, Lu et al. (2018) [2] suggests that the attention has to be directed on aerosol surfaces. Several studies have highlighted the importance of iron(III) carboxylate complexes in the troposphere as chromophores to initiate radical chemistry in aerosol particles involving important atmospheric oxidants, such as ROS [3]. The aim of this work is to assess the involvement of ROS in the conversion of NO<sub>2</sub> into HONO, where ROS are provided by Fe-carboxylate photochemistry. Our first hypothesis is that HO<sub>2</sub> can react with NO<sub>2</sub> leading to HONO through the formation of peroxyxynitric acid (HNO<sub>4</sub>) in aerosol particles [4].

We performed CWFT experiments by exposing a film containing Fe(III)-citrate/citric acid to a highly humidified gas flow containing a low mixing ratio of NO<sub>2</sub>, and irradiating with UV-A lamps to trigger the photochemistry. The gas phase composition was monitored with a chemiluminescence detector (CLD) for NO, an infrared absorption analyser (NDIR) for CO<sub>2</sub> to track Fe(III)-citrate photochemistry [3], and a cavity enhanced absorption instrument (ICAD) for NO<sub>2</sub> and HONO [5]. In order to explore the HONO production mechanism experiments at different pH and NO<sub>2</sub> mixing ratios were performed.

Fig. 1 illustrates the results of a CWFT experiment performed with about 72 ppb of NO<sub>2</sub>. When encountering the film in the dark a small fraction of NO<sub>2</sub> is taken up causing a simultaneous production of HONO. However we can observe that switching on the light enhances this conversion, inducing additional formation of nitrogen monoxide (NO). Considering the actinic flux used in this work, the estimate of the NO<sub>2</sub> photolysis rate suggests that NO<sub>2</sub> photolysis can be neglected, thus NO may come from HONO decomposition in highly acidic conditions [6] or other still not identified processes occurring in the film. The CO<sub>2</sub> signal traces the catalytic cycle of Fe(III)-citrate, as it is produced directly upon Fe(III)-citrate photolysis. It is also a monitor of ROS

production throughout the irradiation time [3]. Interestingly switching off the light does not cause a full recovery of all signals, rather it suggests that intermediates are building up during irradiation that are later continuing to react in the dark.

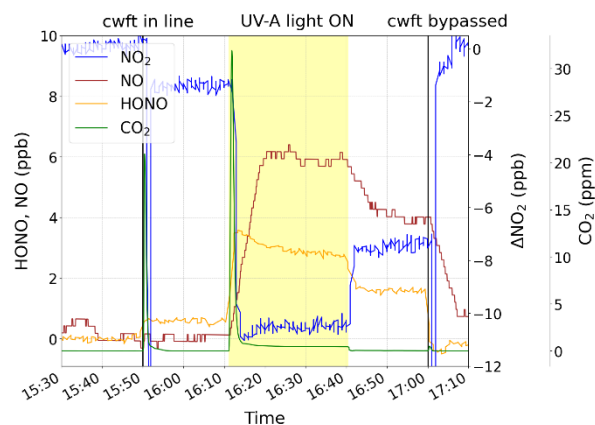


**Fig. 1:** Time profile of NO<sub>2</sub>, HONO, NO and CO<sub>2</sub> during a CWFT experiment. After being exposed to NO<sub>2</sub> the light is turned on triggering the photochemistry within the film.

Preliminary data analysis is not showing a clear correlation between the HONO yield and the NO<sub>2</sub> concentration, which motivates further investigations in order to shed light on the mechanism behind these observations. For this purpose additional experiments adding HSO<sub>3</sub><sup>-</sup> in the film to suppress the peroxyxynitrite pathway are needed. Overall, the results showed that Fe(III)-citrate induces NO<sub>2</sub> conversion into HONO suggesting a possible interplay between Fe-carboxylate photochemistry, ROS and NO<sub>y</sub> chemistry, highlighting the importance of iron complexes in the multiphase chemistry of aerosol particles.

We acknowledge funding from the Swiss National Science Foundation (Grant 188662).

- [1] C. Yu et al., ACS Earth Space Chem., **6**, 1960-1968 (2022).
- [2] X. Lu et al., Environ. Res. Lett., **13** (2018).
- [3] J. Dou et al., Atmos. Chem. Phys., **21**, 315-338 (2021).
- [4] X. Wang et al., Environ. Sci. Technol., (2020).
- [5] M. Horbanski et al., Atmos. Meas. Tech., **12**, 3365-3381 (2019).
- [6] J. Baker et al., Phys. Chem. Chem. Phys., **1**, 683-690 (1999).

## IODINE SPECIATION RESULTING FROM IRON ORGANIC COMPLEX PHOTOLYSIS

L. Iezzi (PSI LUC, ETHZ), M. Reza (PSI LUC, CUB), H. Finkenzeller, R. L. Mauldin (CUB), A. Roose (PSI LUC, PHLAM), T. Bartels-Rausch (PSI LUC), R. Volkamer (CUB, PSI LUC, ETHZ), M. Ammann (PSI LUC)

**Recent studies suggest reduction of iodate to explain recycling of reactive iodine species in the gas phase. Here, we investigate iodine speciation in products of iodate reduction induced by Fe-carboxylate photochemistry.**

The iodine cycle is an important topic in tropospheric chemistry, because of its role in affecting gas phase processes and in new particle formation events [1]. Recent field measurements are showing the prevalence of recycling reactions of reactive iodine species from the condensed phase of aerosol particles to the gas phase [2, 3], suggesting a catalytic nature of the iodine cycle in the troposphere [4]. These recycling reactions may be driven by still not well understood iodate reduction processes. Fe-carboxylate complexes play a key role in multiphase chemistry of aerosol particles due to their capability to initiate free radical chemistry by producing reactive oxygen species (ROS) in the condensed phase [5]. But the role of transition metals in the redox chemistry of iodine has not yet been clarified. The aim of this work is to explore the mechanism of iodate reduction induced by Fe-carboxylate photochemistry by characterizing the iodine speciation ensuing from this chemistry.

We performed coated wall flow tube (CWFT) experiments with aqueous films of iodate and Fe(III) citrate (Fe-cit) using citric acid (CA) as a matrix, which is an established proxy for secondary organic aerosols with well characterized microphysical properties [6]. The CWFT was coupled with a cavity enhanced differential optical absorption (CE-DOAS) instrument in order to detect  $I_2$ , and with a chemical ionization mass spectrometer (CIMS) to detect other iodine species. Both instruments were provided by the University of Colorado in Boulder (UCB). CIMS represents a valuable aid for the scope of this work because of its high time resolution, high sensitivity, and its capability to detect simultaneously many different iodine species [7].

Fig. 1 illustrates the main findings of a photochemical experiment by using visible light. When switching on the light free radical chemistry is triggered by Fe-cit photolysis as we can observe from the  $CO_2$  signal (in green).  $CO_2$  results from decarboxylation occurring immediately after Fe-cit photolysis. Despite the lower quantum yield of Fe-cit for this wavelength range the amount of ROS produced appears to be sufficient to initiate the reduction of iodate within the film.  $I_2(g)$  is the main gas phase product. However, other, both inorganic and organic iodine-species are produced in response to irradiation, implying a complex mechanism involving many different oxidation states of iodine. Furthermore, the time profiles indicate first and second generation products. This result would be in agreement with the

study of Yu et al. 2019 [8], where inorganic iodine represents the majority of iodine in newly formed particles, whereas soluble organic iodine takes over in aged particles. Finally the presence of OVOCs species may come from Fe-cit photochemistry itself [5].

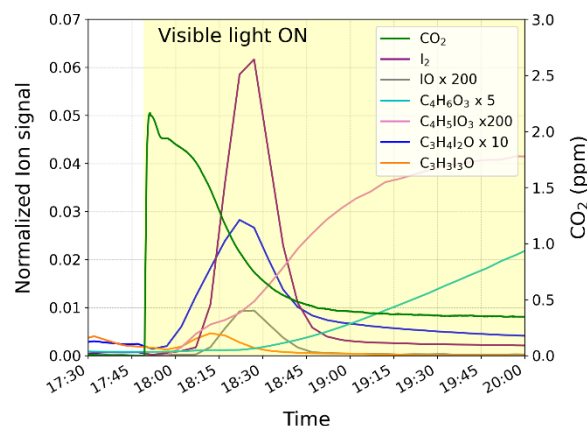


**Fig. 1:** Time profile of iodine species detected by the CIMS and  $CO_2$  detected by a NDIR  $CO_2$  analyzer to track Fe-cit photochemistry. Only few of the 12 species detected are shown in the plot.

In conclusion, visible light seems to be sufficient to efficiently reduce iodate in presence of Fe-carboxylate complexes. Such a mechanism involves different inorganic and organic iodine species, but further studies need to be carried out in order to characterize those species and to shed light on the role of Fe-carboxylates in iodine cycling.

We acknowledge funding from the Swiss National Science Foundation (Grant 188662).

- [1] A. Saiz-Lopez et al., *Chemical Reviews*, **112**, 1773-1804 (2012).
- [2] T. K. Koenig et al., *Proc. Nat. Acad. Sci.*, **117**, 1860-1866 (2020).
- [3] T. K. Koenig et al., *Sci Adv*, **7**, eabj6544 (2021).
- [4] R.-J. Huang et al., *Proc. Nat. Acad. Sci.*, **119**, e2201729119 (2022).
- [5] J. Dou et al., *Atmos. Chem. Phys.*, **21**, 315-338 (2021).
- [6] D. M. Lienhard et al., *J. Phys. Chem. A*, **116**, 9954-68 (2012).
- [7] M. Wang et al., *Atmos. Meas. Tech.*, **14**, 4187-4202 (2021).
- [8] H. Yu et al., *Atmos. Chem. Phys.*, **19**, 4025-4039 (2019).

## THE SURFACE PROPENSITY OF IODINE SPECIES FROM THEORY

A. Roose (PSI LUC), M. Ammann (PSI LUC), M. Krack (PSI LMS)

**Whether atmospheric iodine species are depleted or enhanced at the interface of aqueous aerosol particles is relevant for iodine recycling and thus the ozone budget and climate. Here, we theoretically assess their surface propensity.**

Atmospheric iodine is involved in chemistry that leads to new particle formation [1] and the depletion of ozone [2]. Furthermore, some multiphase recycling mechanisms involving aerosol particles prevent its deposition and increases its lifetime [3]. One relevant piece of information for the understanding of these recycling processes is the surface propensity of these iodine species. Theoretical computations can be used to determine the surface propensity and to compare it to experimental investigations. They can also be used to address species that are short-lived or that cannot be obtained in a range of concentration amenable to experimental investigation. In this work, the surface propensity of  $I^-$ , HOI and  $HIO_3$  has been investigated in a slab of 215 water molecules by AIMD at the revPBE-D3/DZVP-SR level in CP2K [4].

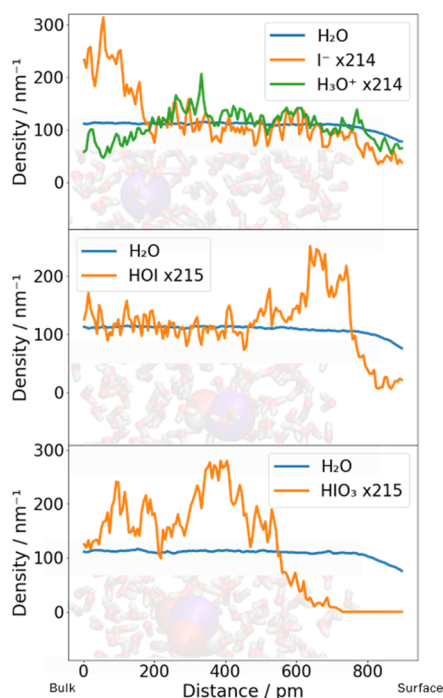


**Fig. 1:** Density profiles of  $I^-$  (top), HOI (center) and  $HIO_3$  (bottom) obtained by AIMD at the revPBE-D3/DZVP-SR level.

Fig. 1 shows the density profiles of the center of mass of iodide, HOI and  $HIO_3$  from the bulk (left) to the surface (right). The density profiles show an evidence of higher surface enrichment in the case of HOI followed by  $HIO_3$ . Contrary to the other two oxides, iodide seems

more bulk active having only a slight depletion at the surface.  $HIO_3$  is enhanced at the sub surface layers but is depleted from the surface layer. Analyses to obtain the free energy profiles are ongoing.

Fig. 2 shows the spatial distribution function (SDF) of water around  $HIO_3$  (left) and HOI (right). The coordination numbers obtained by the radial distribution function indicate that 3 water molecules are in the first solvation sphere of the iodine atom only in the case of  $HIO_3$  (2 are included in the ring on the SDF). In total 6 water molecules are in the first solvation sphere of  $HIO_3$  as a whole, while only 4 are in the first solvation sphere of HOI. Iodide (not shown) has 10 water molecules in its first solvation sphere based on the coordination number. The decreasing number of water molecules in the vicinity of the iodine species is correlated with the increasing surface propensity observed in the density profiles.

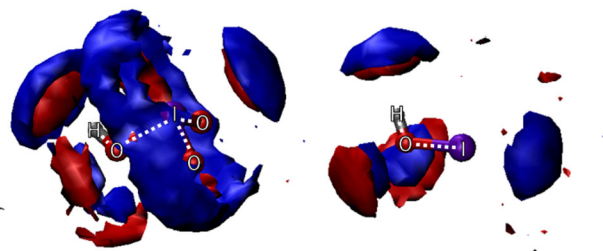


**Fig. 2:** Water (O: red, H: blue) spatial distribution around  $HIO_3$  (left) and HOI (right).

We acknowledge funding from the Swiss National Science Foundation (Grant 188662) and from European Union's Horizon 2020 research and innovation program under the Marie Skłodowska-Curie grant agreement No 884101 (PSI-FELLOW-III-3i). This work was supported by a grant from the Swiss National Supercomputing Center (CSCS) under project ID 447.

- [1] H. Finkenzeller et al., Nat. Chem., **15**, 129-135 (2022).
- [2] A. Saiz-Lopez et al., Chem. Rev., **112**, 1773-1804 (2012).
- [3] T. K. Koenig et al., PNAS, **117**, 1860-1866 (2020).
- [4] T. D. Kühne et al., J. Chem. Phys., **152**, 194103 (2020).

## THE SURFACE PROPENSITY OF IODINE SPECIES FROM LIQUID JET XPS

A. Roose (PSI LUC), A. Boucly (PSI LUC/LEC), H. Yang, L. Iezzi (PSI LUC, ETHZ),  
M. Ammann (PSI LUC), L. Artiglia (PSI LSK/LUC)

**Understanding the surface propensity of iodine species at aqueous solution – air interfaces is important in atmospheric chemistry. Here we use liquid jet X-ray Photoelectron Spectroscopy to determine the surface propensity of iodine species.**

Depth profile measurements help in the constraining of kinetic modelling leading to a better understanding of the chemistry at the interface. Atmospheric relevant iodine species are involved in complex multiphase recycling processes [1-3]. However, their surface propensities are still debated notably in the case of iodide [4-5]. Here, the depth profiles of iodide, iodate and iodic acid have been measured at the SIM beamline of the Swiss Light Source.

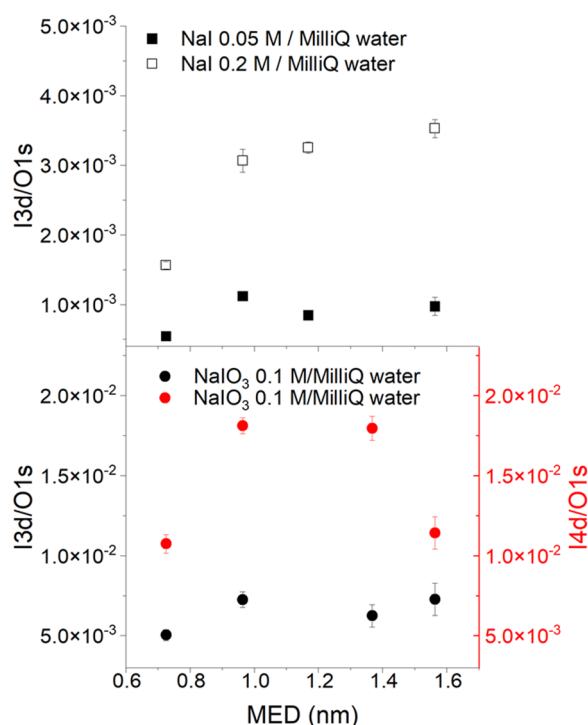


**Fig. 1:** I3d/O1s photoemission signal intensity ratios as a function of the photoelectron mean escape depth (MED) of a 0.05 M and 0.2 M NaI solution (top) and I3d/O1s (bottom black) and I4d/O1s (bottom red) of a 0.01 M NaIO<sub>3</sub> solution. Error bars are 1 $\sigma$ .

Fig. 1 shows the I3d/O1s photoemission signal intensity ratio as a function of the mean escape depth (MED) of photoelectrons from 0.7 nm to 1.6 nm, corresponding to kinetic energies from 210 eV to 510 eV, for NaI and NaIO<sub>3</sub>. Assuming that oxygen atoms exhibit a constant density with depth, the increase of the I3d/O1s ratio in case of iodide clearly indicates a depletion of iodide at the surface of the solution [5]. Concerning the sodium iodate, the depth profiles have been measured using

both the I3d and I4d orbitals. Discrepancies can be observed between the two profiles. In the case of the I3d, the ratio is increasing as we sample deeper in the bulk. The I4d/O1s profiles exhibit a drop at the highest KE, which is not consistent with the I3d/O1s ratio, and a higher value, even though the differences in cross section and photon flux have been accounted for. The reasons for these discrepancies still need to be assessed.

Fig. 2 shows the ratio of HIO<sub>3</sub> and IO<sub>3</sub><sup>-</sup> as a function of the mean escape depth (MED) for different pH conditions (adjusted using H<sub>2</sub>SO<sub>4</sub>) around the pK<sub>a</sub> of the HIO<sub>3</sub>/IO<sub>3</sub><sup>-</sup> couple (0.6, taking into account the ionic strength). In every case, HIO<sub>3</sub> is more surface active than iodate. At pH 1, the ratio tends to the ratio of the acid base equilibrium when sampling deeper in the bulk. For higher pH, the ratios tend to go below the expected equilibrium ratio.

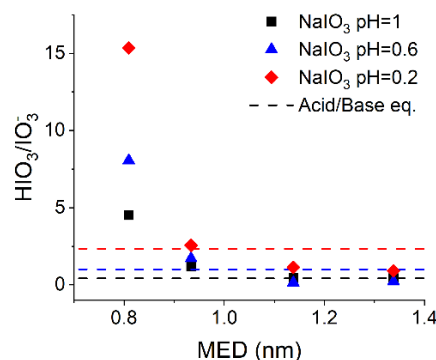


**Fig. 2:** HIO<sub>3</sub>/IO<sub>3</sub><sup>-</sup> ratio (I4d orbital) as a function of the mean escape depth (MED) for three pH conditions. The dashed line represents the ratio based on acid/base equilibrium.

We acknowledge funding from the Swiss National Science Foundation (Grant 188662) and from European Union's Horizon 2020 research and innovation program under the Marie Skłodowska-Curie grant agreement No 884101 (PSI-FELLOW-III-3i).

- [1] H. Finkenzeller et al., *Nat. Chem.*, **15**, 129-135 (2022).
- [2] A. Saiz-Lopez et al., *Chem. Rev.*, **112**, 1773-1804 (2012).
- [3] T. K. Koenig et al., *PNAS*, **117**, 1860-1866 (2020).
- [4] S. Ghosal et al., *Science*, **307**, 563 (2005).
- [5] N. Ottosson et al., **177**, 60 (2010).

## ICE AND CLAY: AN HYDROGEN BONDING INTERPLAY

L. Longetti (PSI LUC), Y. Manoharan (PSI LUC, ETHZ), L. Artiglia (PSI LSK/LUC), D. Pergolesi (PSI NUM), T. Bartels-Rausch (PSI LUC)

**Ice formation is a process of critical importance in atmospheric chemistry. Here we propose an experimental approach to study the interaction of water with manufactured clay layers to gain insights on properties relevant for heterogeneous ice nucleation.**

Clay is one of the major components of atmospheric mineral dust, and it was found to foster heterogeneous ice nucleation [1]. It is still a matter of debate under which conditions the ice formation happens and by means of which mechanism [2]. Focusing on nucleation around clay centers, the interlayer between aluminosilicate building blocks seems to play a pivotal role (Fig. 1). These nanometric interstices may act as condensation pores [3]. Moreover, different cations strongly modify the hydrophilic or hydrophobic properties of such interlayers near the clay-air surface [4]. These processes are linked to the hydrogen-bonding (HB) network, which defines the condensed water structure and also the clay interlayer adhesive forces. We, therefore, aim to investigate the HB network as the strategic player within the presented mechanisms, to gain insights into how the way this interface interacts with water is related to ice nucleation and other chemical and physical processes.

In our research, an epitaxially-grown multilayered aluminosilicate structure is prepared such that a well-characterized clay film could be studied with respect to the role HB has in the interaction at the surface (adsorbates) and within the interlayer channel. An example of this is given in Fig. 1

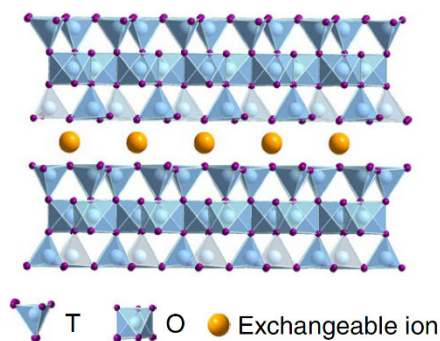


**Fig. 1:** Layered structure of mica clay (side view), composed of octahedral (O) and tetrahedral (T) aluminosilicate planes. In yellow, ions hosted in the interlayer channel are shown (from [5]).

Near-edge X-ray absorption fine structure (NEXAFS) spectroscopy is a still rather uncommon, valuable technique to study the hydrogen bonding network [6]. When electrons are detected, it becomes inherently surface sensitive due to the limited migration of electrons in matter. The experiments were done at the In Situ Spectroscopy (ISS) beamline at SLS, where temperature (T) and relative humidity (RH) can be precisely tuned to

have a sample environment similar to atmospheric conditions [7]. Water adsorption can therefore be studied at varying T and RH. Fig. 2 gives an example of oxygen K-edge NEXAFS spectra of a clay surface with increasing humidity. The signature of adsorbed water with a very flexible hydrogen-bonding structure would appear at around 537 eV [8]. Further investigation will be extended to sub-freezing temperatures and eventually exploit Auger electron spectroscopy, aiming for more contrasted signal from adsorbed water, and XPS to monitor chemical interactions of water with cations on the surface and in the interlayer interstice.

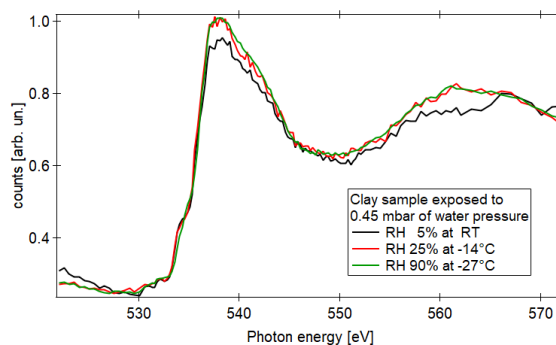


**Fig. 2:** Oxygen K-edge NEXAFS of clay powder for preliminary investigation of water uptake. This shows an increased signal intensity (red and green trace) at the edge, compared to the dry clay (black trace).

We acknowledge funding from the PSI ENE division.

- [1] R. O. David et al., PNAS **116**, 8184-8189 (2019).
- [2] M. A. Freedman, J. Phys. Chem. Lett. **6**, 3850-3858 (2015).
- [3] C. T. Chiou et al., Clays and Clay Minerals **45**, 867-880 (1997).
- [4] M. L. Whittaker et al., PNAS **116**, 22052-22057 (2019).
- [5] Y. Zou et al., Nature Materials **20**, 1677-1682 (2021).
- [6] M. Ammann et al., «X-Ray Excited Electron Spectroscopy to Study Gas-Liquid Interfaces of Atmospheric Relevance», in Physical Chemistry of Gas-Liquid Interfaces, Elsevier. p. 135-166 (2018).
- [7] F. Orlando et al., Topics in Catalysis **59**, 591-604 (2016).
- [8] A. Nilsson et al., J. Electron Spectros. Relat. Phenomena, **177**, 99-129 (2010).

## THE COLD FINGER

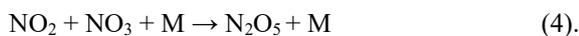
*Y. Manoharan (PSI LUC, ETHZ), A. Laso (PSI LUC), M. Ammann (PSI LUC), T. Bartels-Rausch (PSI LUC)*

**A drawback of spectroscopy studies looking at nitric acid at the air-ice interfacial region is the high concentrations of nitric acid used. Here, we report the development of a set-up that yields low surface coverage of nitric acid on the ice.**

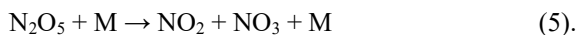
Nitric acid ( $\text{HNO}_3$ ) is one product of nitrogen oxide chemistry in the atmosphere.  $\text{HNO}_3$  is removed from the troposphere by wet and dry deposition contributing to acid rain, and it has been considered as a permanent sink of reactive  $\text{NO}_x$  for a long time. However, on a fundamental basis, there is a lack of understanding of  $\text{HNO}_3$  interaction with water molecules at the air-ice interface and of the photolysis of nitrate and its relevance to atmospheric chemistry. A significant drawback of previous studies is the high concentrations of nitric acid used [1]. High surface coverage can yield different kinetics, product yields, dissociation behavior, and hydrogen bonding network at the interfacial region compared to low concentrations of the contaminant in the ice. The difficulty in achieving low concentrations stems from the fact that  $\text{HNO}_3$  has a low vapor pressure and sticks easily to the walls of the transport line and experimental chamber, hampering a controlled experiment. Therefore, dinitrogen pentoxide ( $\text{N}_2\text{O}_5$ ) was used instead.  $\text{N}_2\text{O}_5$  hydrolyses to  $\text{HNO}_3$  in contact with water or ice surfaces through the following reaction [2],



$\text{N}_2\text{O}_5$  is synthesized by mixing an excess amount of ozone ( $\text{O}_3$ ) with nitrogen monoxide ( $\text{NO}$ ):



Mixing these two gases is straightforward; less simple is the collection of  $\text{N}_2\text{O}_5$  and dosage of it throughout the gas lines and connectors up to the ice sample without losing it due to thermal dissociation,



The home-built set-up, depicted in a simplified scheme in Figure 1, allows synthesis, collection, and the dosage of  $\text{N}_2\text{O}_5$  under clean and stable conditions.

The entire set-up has to be kept extremely dry, such that there is no adsorbed water on surfaces, where  $\text{N}_2\text{O}_5$  could be lost through hydrolysis forming  $\text{HNO}_3$  that would stick to the walls. Therefore, the reactants ( $\text{O}_2$  and  $\text{NO}$  gas) were passed through columns filled with ‘‘Sicapent’’ (phosphor pentoxide,  $\text{P}_2\text{O}_5$ ) to remove water vapor before synthesis. For the synthesis,  $\text{NO}$  and  $\text{O}_3$  were passed through a so-called ‘‘ $\text{N}_2\text{O}_5$  reactor’’, which is a quartz cylinder to form  $\text{N}_2\text{O}_5$ . We preferred to use

quartz instead of glass due to its lower basicity and to reduce losses of  $\text{N}_2\text{O}_5$  to the walls. Next, the  $\text{N}_2\text{O}_5$  was passed through another quartz cylinder ( $\text{N}_2\text{O}_5$  trap), which contains a thin cooled rod in the center, the so-called ‘‘cold finger’’. Decreasing the temperature of the cold finger to below  $-80^\circ\text{C}$  leads to the condensation of  $\text{N}_2\text{O}_5$ . For dosing  $\text{N}_2\text{O}_5$ , the exit of the trap was connected to the experimental chamber by a PFA tube inside a metal bellow, depicted as ‘‘dosing line’’ in Fig. 1. To reduce  $\text{N}_2\text{O}_5$  loss due to thermal dissociation and since its life time increases exponentially with decreasing temperature, the dosing line was cooled.

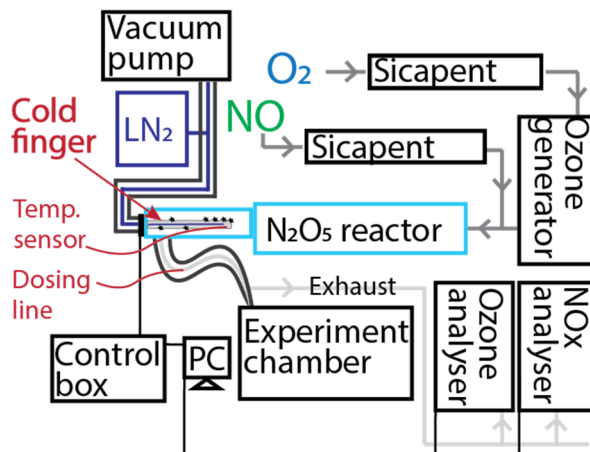


**Fig. 1:** Scheme of the synthesis and collection set-up for dosing  $\text{N}_2\text{O}_5$ . The dosing lines illustrated in dark-grey were made of stainless steel to prevent water vapor diffusion into the dosing lines. Gas lines and the cover of the cold finger consisted of PFA (light-grey lines) due to its inertness towards  $\text{N}_2\text{O}_5$ .

We successfully synthesized  $\text{N}_2\text{O}_5$ , collected it in the trap on the cold finger, dosed the  $\text{N}_2\text{O}_5$  from the cold finger and managed to yield surface coverages of less than a monolayer. This was the most complex in-situ gas-phase synthesis that we have yet coupled to the end station, opening up ample opportunities for future work.

We acknowledge funding from the Swiss National Science Foundation (Grant 178962).

- [1] A. S. McFall et al., *Environ. Sci. Technol.*, **52**, 10 (2018).
- [2] M. J. Tang et al., *Phys. Chem. Chem. Phys.*, **14**, 24 (2012).

## NITRIC ACID DISSOCIATION AT THE AIR-ICE INTERFACE

*Y. Manoharan (PSI LUC, ETHZ), L. Longetti, M. Ammann, T. Bartels-Rausch (PSI LUC)*

**We investigated the dissociation degree of nitric acid ( $\text{HNO}_3$ ) at the interfacial region of ice at  $-30^\circ\text{C}$  and  $-50^\circ\text{C}$ . We aim to contribute to the poorly understood role of interfacial acid-base chemistry on the partitioning of acids to ice.**

High interest in studying the interaction of acids with ice stems from the impact on the composition of the troposphere. Partitioning of nitric acid to ice plays an important role in modifying the nitrogen oxide budget and the hydrogen radical budget affecting the oxidative capacity of the atmosphere. Next to this environmental importance, there is also the fundamental interest in understanding the acid-base concept that is well-known for solutions but cannot be applied to the interface [1]. Previous spectroscopic work of our group [2] revealed that acidic trace gases adsorbed on ice exists in molecular and ionic (i.e., dissociated) form and that the dissociation behavior does not follow the one of a liquid bulk phase.

We aimed to characterize the degree of dissociation of  $\text{HNO}_3$  in the interfacial region of ice upon adsorption at different temperatures. The hypothesis is that the dissociation is driven by the flexibility of the hydrogen bonding network (QLL), which increases with temperature. We performed near-ambient pressure X-ray photoelectron spectroscopy (XPS) experiments at the ISS beamline at the SLS. The analysis chamber was coupled to a home-built set-up for synthesis, crystallization, and dosage of dinitrogen pentoxide ( $\text{N}_2\text{O}_5$ ), which hydrolyses to  $\text{HNO}_3$  in contact with the ice surface [3].

Fig. 1 shows the N1s photoemission spectra acquired on ice in the presence of  $\text{HNO}_3$  at  $-30^\circ\text{C}$  (top) and at  $-50^\circ\text{C}$  (middle) and on MgO in the presence of  $\text{HNO}_3$  and adsorbed water at  $-25^\circ\text{C}$  (bottom). Two main features are visible in each spectrum: A broad feature appears at 407-408eV binding energy upon dosing  $\text{HNO}_3$  to the samples and a sharp feature at 405eV that we assigned to gas-phase  $\text{N}_2$ . All three spectra in Fig.1 show another broad feature at 400-402eV binding energy, labelled with "red-N" for reduced nitrogen species. We assigned it to nitrogen contamination from the chamber and dosing lines since we detected it on clean ice before dosing  $\text{HNO}_3$ . Binding energies (BE) were referenced to the BE of O1s at 533eV.

The N1s spectra of  $\text{HNO}_3$  adsorbed to ice at  $-30^\circ\text{C}$  and to MgO in Fig.1 agree very well. In both spectra, the broad feature at higher binding energy is well fitted by one peak at 406.9eV (assigned to  $\text{NO}_3^-$ ) and a small contribution of a second peak at the shoulder at 407.8eV (assigned to  $\text{HNO}_3$ ). On MgO in the presence of water,  $\text{HNO}_3$  is mainly present in its dissociated form ( $\text{NO}_3^-$ ), as expected from a strong acid adsorbed to a basic

substrate. In contrast, the spectrum of ice at  $-50^\circ\text{C}$  shows a significant contribution of undissociated  $\text{HNO}_3$ . We find only 32% dissociation on ice at  $-50^\circ\text{C}$  but 84% dissociation on ice at  $-30^\circ\text{C}$ . The different dissociation degree is consistent with the temperature increase and more pronounced flexibility in the hydrogen bonding network.

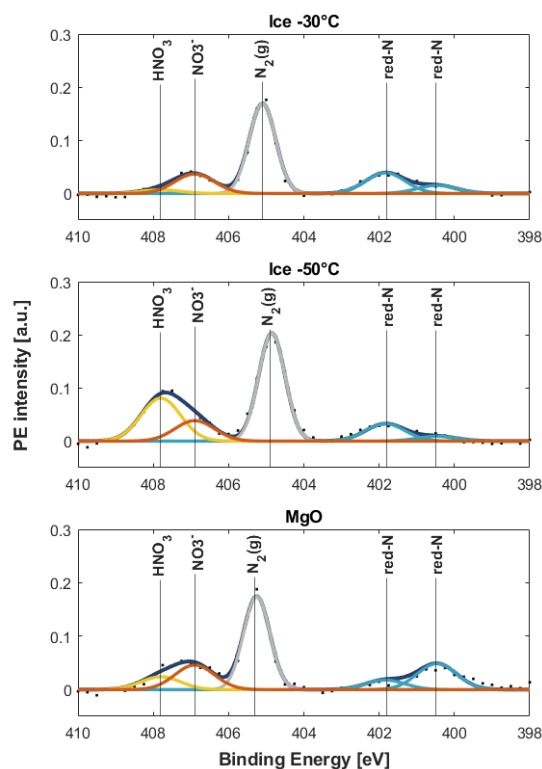


**Fig. 1:** N1s photoemission spectra of the air-ice interface upon adsorption of  $\text{HNO}_3$  on ice at  $-30^\circ\text{C}$  (top), at  $-50^\circ\text{C}$  (middle), and on MgO (bottom), plotted with black dots. The N1s photoemission signal is deconvoluted in five Gaussians: Undissociated  $\text{HNO}_3$  (yellow), dissociated nitric acid  $\text{NO}_3^-$  (red),  $\text{N}_2$  gas phase (grey) and nitrogen contamination (light blue); The total fit is shown in dark blue.

We acknowledge funding from the Swiss National Science Foundation (Grant 178962).

- [1] S. Zimmermann et al., *Phys. Chem. Chem. Phys.*, **18**, 13799-13810 (2016).
- [2] T. Bartels-Rausch et al., *ACS Earth Space Chem.*, **1**, 572-579 (2017).
- [3] Y. Manoharan et al., *LUC Annual Report*, this volume, p. 14.

## ACID-BASE CHEMISTRY OF AMMONIA AT THE ICE-VAPOR INTERFACE

C. Richter, S. Gholami (FHI), Y. Manoharan (PSI LUC, ETHZ), T. Buttersack (FHI), L. Longetti (PSI LUC), L. Artiglia (PSI LSK/LUC), M. Ammann, T. Bartels-Rausch (PSI LUC), H. Bluhm (FHI)

**The acid-base equilibrium at aqueous interfaces is of profound importance to atmospheric chemistry. Here, we report on the adsorption and dissociation of the inorganic base ammonia ( $\text{NH}_3$ ) at the air-ice interface.**

Ambient pressure X-ray photoelectron spectroscopy (APXPS) has been established as an important technique for investigating liquid-vapor and ice-vapor interfaces [1]. For environmental and atmospheric science, APXPS is particularly useful for studying the chemical composition of the interface and interrogating the chemical state of the solutes and adsorbates. This investigation focused on the adsorption of gas-phase  $\text{NH}_3$  to the ice surface at different temperatures and determining its protonation state.  $\text{NH}_3$  is an atmospheric trace gas recently recognized for its role in producing atmospheric particles in Arctic environments [2]. In aqueous environments,  $\text{NH}_3$  is in equilibrium with its conjugate acid  $\text{NH}_4^+$  (ammonium) [3]; both species are distinguishable in APXPS.

Using the NAP-XPS endstation at the ISS beamline of the SLS, ice samples were prepared at  $-29^\circ\text{C}$  and  $-45^\circ\text{C}$  and subsequently exposed to a stream of  $\text{NH}_3$  diluted in argon as carrier gas. The uptake of  $\text{NH}_3$  was monitored by recording N1s and O1s spectra during the increase of the  $\text{NH}_3$  partial pressure to approximately  $10^{-3}$  mbar in the experimental chamber. Once the N1s signal stabilized, the chemical state of  $\text{NH}_3$  at the ice surface was investigated in more detail. Preliminary results of this investigation are depicted in the N1s core level spectra in Fig. 1, with experimental data shown as black symbols and fits to the data as red traces. The individual contributions to the fit consist of unknown nitrogen contamination (orange trace) and adsorbed ammonia (blue trace). A tentative analysis based on ammonia photoemission work in aqueous environments allowed the identification of two species at the ice surface, i.e.,  $\text{NH}_3$  and  $\text{NH}_4^+$  [4, 5]. At  $-29^\circ\text{C}$ , the fraction of  $\text{NH}_4^+$ , i.e., the degree of protonation was approximately 40 %, whereas, at  $-45^\circ\text{C}$ , no protonation could be detected. This observation suggests a temperature-induced shift in the acid-base equilibrium at the  $\text{NH}_3$ -ice interface.

In addition, preliminary experiments on  $\text{CH}_3\text{COOH}$  (acetic acid) and  $\text{NH}_3$  co-adsorption were performed at  $-29^\circ\text{C}$  (Fig. 1 (c)). In these experiments, an increased fraction of adsorbed ammonia on the ice surface was present as  $\text{NH}_4^+$  ( $\approx 63\%$ ), indicating a further shift in the acid-base equilibrium induced by the presence of the organic acid. The next round of experiments will focus on gathering a comprehensive data set on the interfacial interaction of  $\text{NH}_3$  with co-adsorbates at the ice surface.

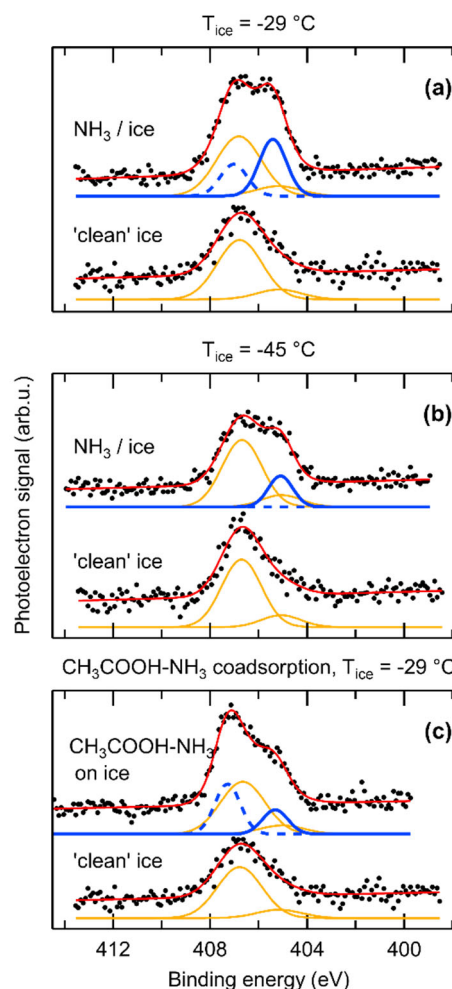


**Fig. 1:** N1s core-level spectra of the  $\text{NH}_3$ -ice interface at  $h\nu = 650$  eV and (a)  $-29^\circ\text{C}$  and (b)  $-45^\circ\text{C}$ . (c) N1s core-level spectra of the  $\text{CH}_3\text{COOH}$  and  $\text{NH}_3$  co-adsorbed at the ice-vapor interface at  $-29^\circ\text{C}$ .

YM acknowledges funding from the Swiss National Science Foundation (Grant 178962) and SG from the IMPRS-EPPC of the Max Planck Society.

- [1] R. Dupuy et al., *J. Chem. Phys.*, **154**, 060901 (2021).
- [2] B. Croft et al., *Nat. Commun.* **7**, 13444 (2016).
- [3] H. Ogasawara et al., *J. Chem. Phys.* **112**, 8229-8232 (2000).
- [4] I. Unger et al. *J. Phys. Chem. B* **119**, 10750-10759 (2015).
- [5] J. Werner et al. *J. Phys. Chem. B* **118**, 7119-7127 (2014).

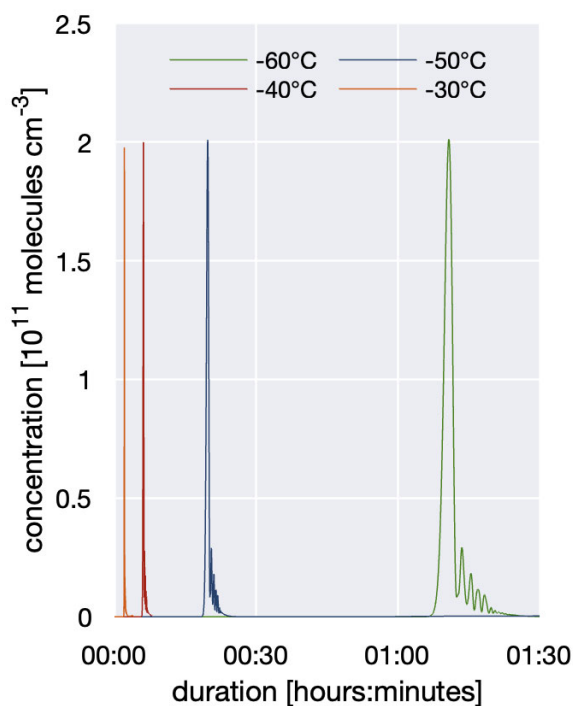
## MODELLING CHEMISTRY IN SNOW

*T. Bartels-Rausch (PSI LUC), J. Thomas (Univ. Grenoble), J. Stutz (UCLA)*

**Atmospheric 1-D process models simulate the impact of chemistry on the composition in the boundary layer. They are a valuable tool for interpreting field observations and testing specific processes in a controlled manner.**

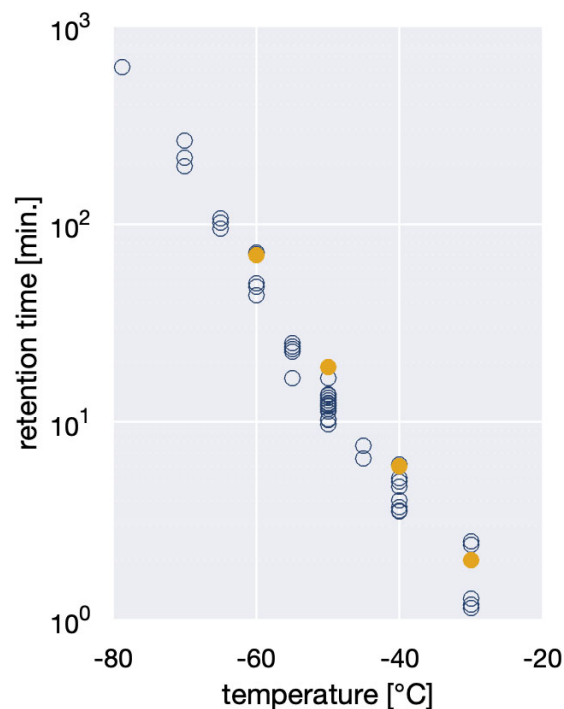
In this work, a complete description of snow–air interactions was developed and added to an existing 1-D atmospheric process model, PACT-1 [1]. The PACT-1D model was recently successfully used to simulate vertical profiles of nitrogen oxide chemistry in a Southern California early summer urban environment. The PACT-1D model parameterizes atmospheric emissions, gas-phase and aerosol chemistry in the atmosphere, transport, and mixing.

Fig. 1 shows the simulation results of the wind-driven transport of acetone through a specific snow sample. The model explicitly treated the resistance of trace gas transport by the porosity of snow and the finite residence time of the trace gas when adsorbed to the snow surface. In these experiments,  $2 \times 10^{11}$  molecules  $\text{cm}^{-3}$  acetone were dosed to the snowpack at 66 cm depth and at time 0 min.



**Fig. 1:** PACT-1D simulation results of acetone transport through a 66 cm long snowpack at a constant wind speed of  $500 \text{ ml min}^{-1}$ . Duration defines the time that acetone requires to pass the entire snowpack. The oscillations are numerical artefacts.

The simulation captures the slower transport of acetone through the snow with decreasing temperatures. Developing the PACT-1D, transport in the snow was introduced based on a detailed physicochemical description derived from laboratory experiments [2-4]. These model runs were set up to reproduce laboratory studies with well-characterized snow properties and wind velocities in the snow. The results in Fig. 2 show excellent agreement giving confidence in the parameterization of transport through the snow in the model. The slight overestimation of the retention time might be due to uncertainties in the physical snow parameters of the snow used during the experiments.



**Fig. 2:** Comparison of the simulated retention time of acetone transport through snow (filled yellow circles) with laboratory results (open blue circles).

We acknowledge funding from the Swiss National Science Foundation (Grant IZSEZ0\_210264).

- [1] K. Tuite et al., *J. Geophys. Res.*, **126**, e2021JD034689 (2021).
- [2] C. Guimbaud et al., *Int. J. Mass Spec.*, **226**, 279-290 (2003).
- [3] F. Dominé et al., *Atmos. Chem. Phys.*, **8**, 171-208 (2008).
- [4] T. Bartels-Rausch et al., *Atmos. Chem. Phys.*, **13**, 6727-6739 (2013).

## RECENT DECREASE IN HEAVY METAL POLLUTION FROM THE FSU REGION

A. Eichler (PSI LUC), P. Nalivaika (PSI LUC, Univ. Bern), T. M. Jenk (PSI LUC), T. Singer (PSI LUC, Univ. Bern), S. Kakareka, T. Kukharchyk (INM Minsk), S. Eyrikh, T. Papina (IWEPI), M. Schwikowski (PSI LUC, Univ. Bern)

**Altai ice cores show vast anthropogenic heavy metal perturbations during the period 1940-2018 from the FSU region, peaking in the 1970s. The magnitude of decreasing emissions between 1975 and 2015 between ice core concentrations and new emission estimates agrees for Cu, Sb, Zn, but differs for Bi, Cd, Pb.**

Atmospheric heavy metal (HM) pollution caused by metal smelting, mining, and fossil fuel combustion from the territory of the former Soviet Union (FSU) considerably influenced atmospheric concentrations of HM and presented a significant issue for human health and the environment, especially during the 1970s. Due to scarce monitoring data and fragmentary reporting, FSU emission levels are not well understood and existing ice core records and expert emission estimates revealed an opposing trend in the recent ~30 years [1,2].

Here we present records of post-Soviet Union anthropogenic HM (Bi, Cd, Cu, Pb, Sb, Zn) emissions and their significance compared to the Soviet Union times based on three available ice cores from the Mongolian Altai (Tsambagarav ice core, period 1710-2009 AD) and Siberian Altai (Belukha ice cores, period 1680-2018 AD). The major source region of air pollution arriving at the Altai is primarily the territory of the FSU except for the eastern-most Siberian parts. Reconstructed trace element records were complemented with new expert HM emission estimates (1975-2015 AD) to establish a robust trend of recent FSU HM emissions. The non-dust HM concentrations were calculated accordingly to  $[HM]_{\text{non-dust}} = [HM] - [HM]/[Ca]_{\text{preind}} \cdot [Ca]$  using the pre-industrial  $[HM]/[Ca]$  ratio for the period

1710-1780. 10-year ice-core HM concentration means were averaged for all three cores (Fig. 1) and compared with new emission estimates [3]. The ice-core composites reveal low preindustrial values 1700-1940 AD and an overwhelming anthropogenic impact 1940-2018 predominantly from leaded gasoline, fossil fuel combustion and nonferrous/iron and steel metallurgy on the territory of the FSU. All HM concentrations peak in the 1970s. Consistent with the emission estimates ice-core concentrations of Cu, Sb, Zn decrease steadily afterwards and their 2010s levels correspond to 20-40% of the maximum values in the 1970s and are comparable to the 1940s-1950s levels. A similar magnitude was also proposed for the decrease in Bi, Cd, Pb, however, ice-core concentrations in 2015 still correspond to 50-70% of their 1975 levels. This is probably due to an underestimation of recent emissions from fossil fuel combustion and/or metallurgical processing. Nevertheless, the clear decrease in most of the HM concentrations after the 1970s indicates that opposing recent trends observed at some Central Asian sites are not related to growing emissions from the territory of the FSU, but from China [4].

We acknowledge funding from the Swiss National Science Foundation (Grant 181985).

- [1] B. Grigholm, et al., *Atmos Environ*, **131**, 17 (2016).
- [2] HELCOM, <http://www.helcom.fi/>.
- [3] S. Kakareka et al., *LUC Annual report*, **29** (2022).
- [4] H. Z. Tian et al., *ACP*, **15**, 10127 (2015).

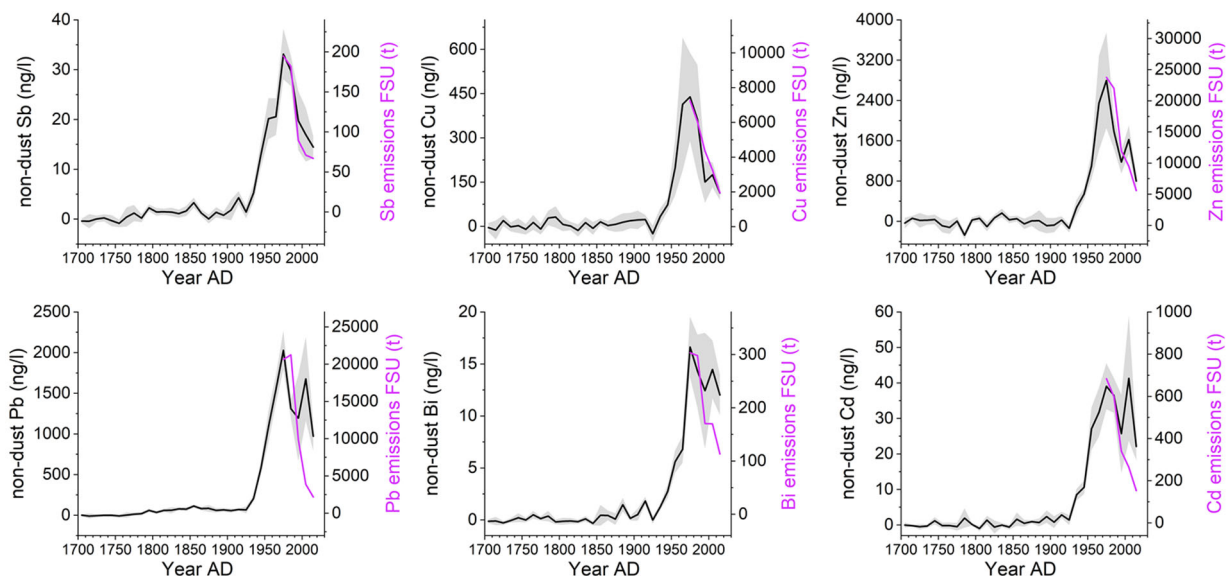


**Fig. 1:** Comparison of 10-year Altai ice-core HM composites (period 1700-2018, black lines, gray ranges represent the  $\pm 1\sigma$  standard error) and emission estimates for the FSU (period 1975-2015, pink lines) for Bi, Cd, Cu, Pb, Sb, Zn.

## ANALYSIS OF TRACE ELEMENTS IN GLACIER ICE WITH ICP-TOF-MS

*T. S. Münster (PSI LUC, Univ. Bern), T. M. Jenk, A. Eichler (PSI LUC), G. Lee (Univ. Bern),  
M. Schwikowski (PSI LUC, Univ. Bern)*

**Trace element (TE) concentrations determined with two different instruments (ICP-SF-MS and ICP-TOF-MS) in sections of a Colle Gnifetti ice core showed overall good agreement for 33 out of the 35 TE analyzed.**

Trace elements (TE) in glacier ice reflect the composition of deposited aerosols and thus allow determining their origin, e.g. from oceans (sea salt), desert areas (mineral dust), volcanoes and anthropogenic pollution. However, TE analysis in ice cores is a challenge because they are present in dissolved and particulate form. For determining TEs in ice cores, inductively coupled plasma mass spectrometry (ICP-MS) has been the method of choice, either using a quadrupole or sector field MS. Recently, an ICP time of flight (TOF) MS was introduced for TE analysis, which has a much faster scan time for a full element spectrum (2 ms) than previously used techniques. Thus, it may allow single particle analyses and high spatial resolution in ice cores using continuous ice melting applications [1].

To characterize the performance of the new ICP-TOF-MS (icpTOF R, TOFWERK AG, Thun, Switzerland) compared to the established ICP-SF-MS (Element 2, Thermo Fisher Scientific, Bremen, Germany), we used parallel ice core samples from a shallow ice core drilled on Colle Gnifetti glacier (Swiss Alps) in 2021 [2]. The samples were acidified with ultrapure HNO<sub>3</sub> to a final concentration of 0.2 M with the same short time (1.5 min) [3, 4]. Additionally, we added a desolvating nebulizer (Apex Omega) to the inlet-system of the ICP-TOF-MS. Unlike the before used cooled spray chamber, the Apex produces a dry aerosol. As a result, we increased the sensitivity of the ICP-TOF-MS by a factor of five to ten. This sensitivity improvement leads to a decrease of the detection limit for most elements.

TE concentrations of parallel ice core samples determined with the ICP-SF-MS and the ICP-TOF-MS showed close agreements in trends, averages and Pearson correlation coefficients for soluble as well as insoluble TE, see concentrations of Eu as example in Fig. 1. For 33 (Na, Al, Ca, V, Cr, Mn, Fe, Co, Ni, Cu, Zn, Rb, Sr, Zr, Mo, Ag, Cd, Sb, Cs, Ba, La, Ce, Pr, Nd, Sm, Eu, Yb, W, Tl, Pb, Bi, Th, U) out of the 35 TE analyzed, the difference in average concentration was below 10 %. Just two isotopes showed a difference over 10 % (Mg: 10-20%, Sc: >40%). The Pearson correlation coefficients were above 0.9 for 32 TE (see example in Fig. 1).

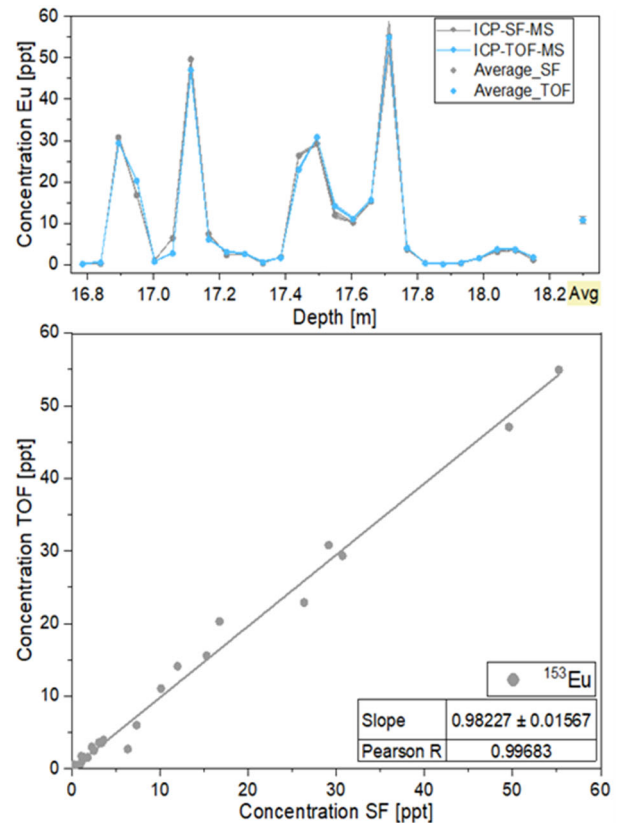


**Fig. 1:** Top: Records of Eu concentrations determined with ICP-SF-MS and ICP-TOF-MS in a section of the Colle Gnifetti ice core. Average concentrations (Avg.) of all samples are displayed in the right. Bottom: Scatter plot, regression line and Pearson coefficient of Eu concentrations determined with ICP-SF-MS and ICP-TOF-MS in the same section of the Colle Gnifetti ice core.

In summary, we were able to reach a good comparability of the analyzed TE concentrations for over 94% of the elements. Why this is not the case for Mg and Sc is the topic of ongoing research.

- [1] T. Erhardt et al., *Environ. Sci. Technol.* **53**, 13275-13283 (2019).
- [2] T. M. Jenk et al., *LUC Annual Report*, p. 23 (2021).
- [3] T. S. Münster et al., *LUC Annual Report*, p. 33 (2019).
- [4] T. S. Münster et al., *LUC Annual Report*, p. 29 (2020).

## PRE-INDUSTRIAL TO INDUSTRIAL CHANGES OF ORGANIC AEROSOLS

*T. Singer (PSI LUC, Univ. Bern), T. M. Jenk, F. Burgay (PSI LUC), J. Strähl, S. Szidat (Univ. Bern), M. Schwikowski (PSI LUC, Univ. Bern)*

### Long-term records of organic aerosols from the Colle Gnifetti ice core show distinctly different trends of the fossil and non-fossil fraction.

The impact of anthropogenic aerosols on cloud droplet concentrations and radiative properties is the source of one of the largest uncertainties in the radiative forcing of the climate during the industrial period. Most of these uncertainties are due to insufficient knowledge about the composition and extent of natural emissions before the onset of industrialisation [1].

Atmospheric organic aerosol (OA) is the dominant component that accounts for a large proportion (20-70%) of particulate matter [2] and causes numerous environmental, health and climate issues [3]. OA is either directly emitted from vegetation, fossil fuel, and biomass burning (primary OA) or formed as secondary particles through the photochemical conversion of volatile organic compounds (VOC) [4] and can be altered due to interactions of biogenic VOC with anthropogenic emissions such as  $\text{NO}_x$  and  $\text{SO}_2$  [5].

OA can be divided into water-soluble organic carbon (WSOC) and water-insoluble organic carbon (WIOC). WIOC consists predominantly of primary organic aerosol, whereas WSOC is mainly composed of secondary organic aerosol (SOA) [4]. OA can be further distinguished according to its source. This distinction is possible by radiocarbon ( $^{14}\text{C}$ ) analysis, i.e., by determining the isotopic  $^{14}\text{C}/^{12}\text{C}$  ratio.  $^{14}\text{C}$  analysis is a powerful tool, not only for dating, but also allows a clear distinction between fossil and biogenic (non-fossil) sources of OC. The subsequent radiocarbon source apportionment identifies air pollution sources and quantifies their contribution to air pollution [6].

Alpine glaciers provide access to samples representing past climate and atmospheric conditions and are especially suitable archives for reconstructing the effects of industrialisation, due to their proximity to aerosol sources. We developed a setup that allows the extraction of both WIOC and WSOC fractions from a single ice sample [7]. In the first step, physical filtration of the particles collects the WIOC on a quartz filter, and in the second step, photochemical oxidation of the WSOC leads to its determination based on the  $\text{CO}_2$  produced. The subsequent radiocarbon analysis was performed at the Laboratory of Radiocarbon Analysis in Bern (LARA) using a MIni CARbon DAting System (MICA-DAS).

We applied our method to an ice core from Colle Gnifetti glacier (4455 m a.s.l.), which records mainly a summer signal due to strong vertical transport in summer and loss of light winter snow due to wind erosion in winter.

From 1550 to 1990 CE, the concentration of non-fossil

OC showed some variability with a recent increase starting 1940. The variability is most likely caused by temperature variations, which positively affect biogenic productivity (Fig. 1 top). The concentration of fossil OC, emitted either directly from fossil fuel combustion (e.g. motor vehicles, power generation) or formed as SOA from fossil VOC emissions, has increased since the beginning of the 20<sup>th</sup> century as a result of a progressively intense consumption of fossil fuels in central Europe. Peak values occurred in the 1970s, reflecting increased use of liquid fuels. This is supported by similar trends in concentrations of fossil OC and sulphate and nitrate, which are tracers of fossil fuel consumption and high temperature combustion, respectively (Fig. 1 bottom).

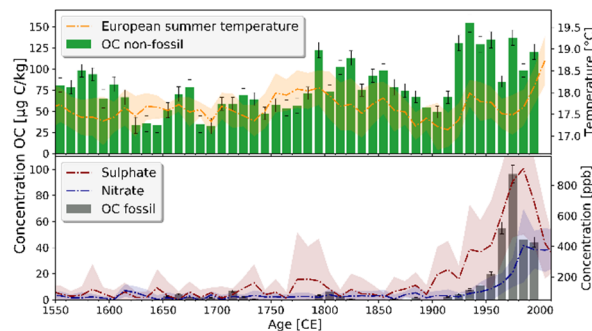


**Fig. 1:** Concentration records of non-fossil OC together with the average European summer temperature [8] (top) and of fossil OC with sulphate and nitrate concentrations (bottom) (10-year averages).

We acknowledge funding from the Swiss National Science Foundation (Grant 200021\_182765).

- [1] K. S. Carslaw et al., *Nature*, **503**, 67-71 (2013).
- [2] J. L. Jimenez et al., *Science*, **326**, 1525 (2009).
- [3] B. Brunekreef et al., *The Lancet*, **360**, 1233-1242 (2002).
- [4] A. Gelencsér et al., *J. Geophys. Res.*, **112** (2007).
- [5] C. R. Hoyle. *Atmos. Chem. Phys.*, **11**, 321-343 (2011).
- [6] S. Szidat et al., *Nuclear Instr. and Methods in Physics Research Section B*, **223-224**, 829-836 (2004).
- [7] T. Singer et al., *LUC Annual Report*, p. 26, (2021).
- [8] J. Luterbacher et al., *Science*, **303**, 1499-1503 (2004).

## FIRST GLANCE AT RECENT ORGANIC RECORD ON GRAND COMBIN

*C. J. Huber (PSI LUC, Univ. Bern), F. Burgay, A. Eichler, T. M. Jenk (PSI LUC), D. Salionov, S. Bjelić (PSI LBK), M. Schwikowski (PSI LUC, Univ. Bern)*

**Here we report on a first application of a novel organic tracer analysis method on a firn core from the Swiss Alps.**

Ice cores from mountain glaciers are valuable natural archives, which allow reconstruction of the composition of the Earth's atmosphere. Until today, mostly the inorganic atmospheric aerosol fraction has been studied; in contrast, the organic aerosol composition is less understood. So far, organic aerosols in ice cores have mainly been reported as bulk parameters (e.g., water insoluble or dissolved organic carbon) or as specific tracers (e.g., biomass burning tracers).

A novel method for the analysis of organic tracers, which was described in previous reports [1, 2], was applied to a firn core drilled on Grand Combin in 2020 (GC20). The firn core was dated applying annual layer counting using stable isotopes ( $\delta^{18}\text{O}$ ) and concentrations of ammonium [3]. During the interpretation of the major ion record, we observed melting effects. This gave us the opportunity to analyze the extent of melt effects on organic aerosol tracers.

In this study, we applied non-target screening (NTS) as well as targeted analysis to the firn core GC20 using high-resolution mass spectrometry. The core was cut in a monthly resolution, in order to investigate seasonality. In a first step, we evaluated the targeted species, which are selected biomass burning tracers vanillin (VAN), vanillic acid (VA), syringic acid (SyAH), syringaldehyde (SyA) and p-hydroxybenzoic acid (PHBA), as well as the biogenic emission tracer pinic acid (PA).

This is the first application of the method to firn samples in a monthly resolution, where we show that we can detect all six species (Fig. 1).

PA and PHBA were detected in most samples and concentrations show large variations, possibly related to seasonality. In contrast, concentrations of VAN, VA, SyA, and SyAH were mostly below the detection limit. For PA we observe a possible effect of melting. The youngest samples show a high concentration and a seasonal cycle, however samples further back in time have a much lower concentration with almost no seasonal variation. For the biomass burning tracers we can also observe a possible influence of melting. The intensity of the peaks in the younger samples are larger than in the older samples. However, the interpretation is not straightforward, as fire events do not occur regularly and may also have a time trend.

The interpretation of all the data generated from the targeted analysis as well as the NTS are still on going.

We acknowledge funding from the Swiss National Science Foundation (Grant 200021\_182765). We would like to thank the ice core drilling team.

- [1] F. Burgay et al. LUC Annual Report, p. 27 (2020).
- [2] F. Burgay et al. LUC Annual Report, p. 28 (2021).
- [3] C. J. Huber et al., LUC Annual Report, p. 25 (2020).

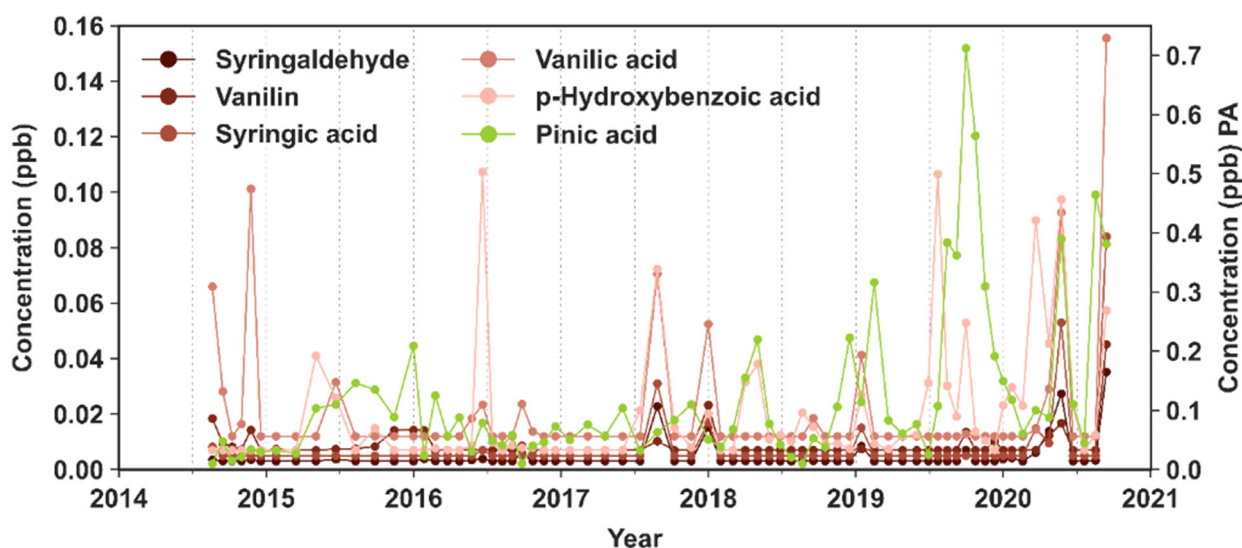


**Fig. 1:** Concentration record for biomass burning tracers (VAN, VA, SyAH, SyA and PHBA) as well as the biogenic emission tracer PA with a monthly resolution from the Grand Combin firn core.

## INSIGHTS FROM THE NON-TARGET ANALYSIS OF THE BELUKHA ICE CORE

F. Burgay (PSI LUC), D. Salionov, S. Bjelić (PSI LUK), C. J. Huber (PSI LUC, Univ. Bern),  
A. Eichler (PSI LUC), T. Singer, M. Schwikowski (PSI LUC, Univ. Bern)

**The application of non-target screening (NTS) methods on ice core samples enables the characterization of a wider suite of compounds, contributing to a more comprehensive understanding of the past atmospheric composition. Here, we present the first insights from the NTS analysis from the Belukha ice core that allowed the identification of 313 different compounds.**

Organic analytical methods applied on ice cores have been mainly focused on targeting specific molecules, such as biomass burning tracers (levoglucosan, lignin degradation products), marine phytoplankton oxidation products (methanesulphonic acid) and low-molecular weight carboxylic acids. However, these compounds only represent a small fraction of the overall organic burden preserved in ice core samples, meaning that the identity of the large majority of the compounds remains largely unknown and not characterized. Today, the availability of high-resolution mass spectrometers unlocks the possibility to explore a wider chemical space through the application of suspect screening (SUS) and non-target screening (NTS) workflows (Fig. 1).

As described in previous reports [1], a novel method for NTS analysis of ice cores was developed and applied on 50 meters of the Belukha ice core (Siberian Altai, 4072 m. a.s.l.) covering a period from approximately 1750 to 1980, embracing both the pre-industrial and industrial periods. The sampling site is influenced mainly by terrestrial biogenic emissions, especially from herbs and conifers [2]. Being located far from the anthropogenic emission sources, the location is less influenced by pollution compared to other glaciers (e.g. Colle Gnifetti in the European Alps). Nevertheless, a significant increase in sulphate concentration (i.e. a proxy for the combustion of fossil fuels, mainly coal and oil) has been observed since 1950s.

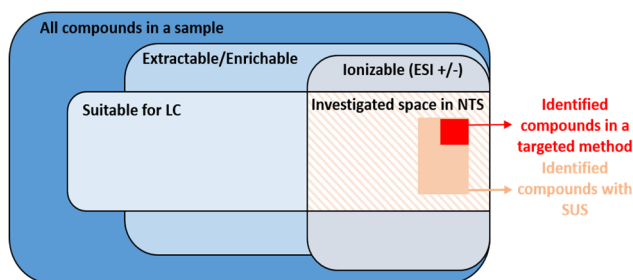


**Fig. 1:** The application of NTS (dashed orange rectangle) and SUS (orange rectangle) approaches enables the possibility to investigate a wider chemical space than standard target methodologies (red rectangle).

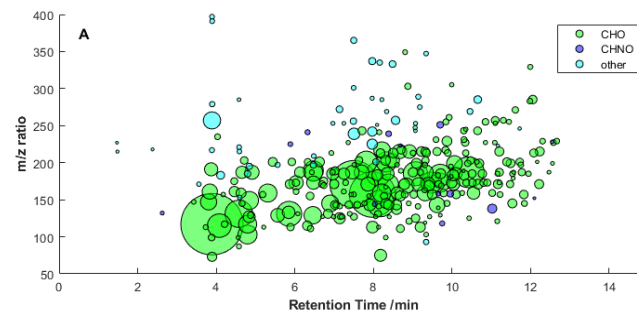


**Fig. 2:**  $m/z$  ratios plotted against the retention time. The size of the circles is proportional to the area of the molecular ions. Green circles refer to CHO compounds, violet circles to CHNO compounds, light-blue circles to compounds defined as “other”.

Here, we present the first NTS results from a Belukha ice sample (dated to 1934) to show the potential that this methodology has for detecting hundreds of different molecules from a single sample and for achieving a broader and more comprehensive understanding of the past atmospheric composition. The results show that up to 313 different compounds were detected, the majority of them (80%) composed of carbon (C), hydrogen (H) and oxygen (O) consistent with the pristine atmospheric conditions present at that time (Fig. 2). 7% of the molecules contains also nitrogen (N) in their structure, while the remaining 13% contains other heteroatoms. The Van Krevelen and Kroll diagrams (not shown) classify the majority of these compounds as semi-volatile and low-volatile oxidation products of monoterpenes, with few of them presenting aromatic features. For their identification, we selected the compounds that have intensities higher than  $3E8$ . We characterized them through the comparison of the  $MS^2$  spectra with the mzCloud spectral library, through the comparison between the retention times (RTs) of the compound candidates and the RTs of the respective standards. 5 out of 10 compounds (all CHO molecules) were identified at Level 1 of the *Schymanski scale* [3], i.e. succinic acid, glutaric acid, azelaic acid, levulinic acid and methylsuccinic acid, which are all typical dicarboxylic acids commonly found in atmospheric aerosol. Among the most abundant CHNO compounds, we identified *p*-nitrophenol that is a biomass burning tracer.

We acknowledge funding from the Swiss National Science Foundation (Grant 200021\_182765).

- [1] F. Burgay et al., LUC Annual Report, p. 27 (2020).
- [2] A. Eichler et al., QSR, **30**, 1027-1034 (2011).
- [3] E. Schymanski et al., ES&T, **48**, 2097-2098 (2014).

## BOREHOLE HORIZONTAL DISPLACEMENT AS A TOOL FOR ICE CORE DATING?

*T. M. Jenk (PSI LUC), P. Gabrielli (UNITO)*

**Dating natural archives like ice cores is fundamental to put the analyzed climate and environmental proxies into a temporal context. Ideally, a combination of different dating methods and modeling is applied.**

Each glacier is a complex system with unique topography and geometry. Aside from geometric characteristics, the dynamics of the ice, which behaves like a viscous fluid, also depend on factors like temperature and precipitation. Temperatures within the archive are inhomogeneous, vertically from surface to bedrock as well as from the accumulation zone down-slope to the glacier tongue at lower elevation. While temperature is important, the amount of snow deposited in the accumulation zone, which as well relates to (air) temperature, has a major effect on the overall glacier mass balance. Both temperature and snow deposition fluctuate over time, resulting in changes to the glacier's mass balance (thus geometry and extent), physical properties of the ice, and consequently ice-flow dynamics. Hence, a glacier is best described as a non-steady state system.

Typically, ice cores are extracted from the accumulation zone where stationary ice frozen to the bedrock and the flow of the layers above causes horizontal shear and thus exponential thinning of annual layers with depth. Achievable resolution of bedrock topography (in steady state) and unknown, past variations in the aforementioned factors controlling ice-dynamics (non-steady state), are the major limitation to model the age of these layers, even with advanced glaciological 3D models [1]. For high-alpine sites, the only absolute method to determine their age is by  $^{14}\text{C}$  dating of the entrapped organic carbon from carbonaceous aerosols [2]. In the upper sections of the core, where layer thickness allows for sufficient resolution, dating based on annual layer counting is usually possible. By combining these methods, an age scale from surface to bedrock can be obtained, but to achieve a continuous chronology, an age model is still needed. It can be based on statistical methods like Monte Carlo simulation or, preferably, also incorporate basic physics laws. Focusing on the vertical column below a defined spot on the glacier and with the constraint of age available from dating, simplified 1D ice-flow models are an option for this purpose [2]. With fewer parameters and of lower mathematical complexity than 3D models, they are computationally efficient for tuning, e.g. by fitting to the dated layers. In addition, inverse modelling approaches, which allow consideration of non-steady state and benefit from the archived information at the same time, become feasible [e.g. 3].

Here, instead of relying on the age of dated layers, we made use of the relative horizontal displacement in the borehole measured with an inclinometer over a 43-day period in the borehole of the Ortles ice core [4]. The

data served as a constraint for the 1D model from Dansgaard and Johnsen (D-J) [5]. The D-J model simplifies ice dynamics within a vertical column, reducing it to four key parameters: ice thickness ( $H$ ), depth ( $z$ ), mean annual accumulation rate ( $b$ ), and shear zone thickness ( $h$ ). Using this model, the relation to time (age at depth  $z_i$ ) can be derived by integrating vertical velocity over depth. To account for the incompressibility of ice, the velocity component resulting from densification of snow to firn and ice was here considered by strictly using units of meter water equivalent (m w.e.; derived from ice core densities), both for modelling and measurements. From the optimal value of  $h$  as a best fit between observed and modeled horizontal flow velocity  $v_x$  (for steady state), a first estimation for  $h$  at high-alpine sites, approximately at the firn-ice transition depth, was obtained. The agreement in overall shape between modelled and observed  $v_x$  is remarkable (Fig. 1). Next, using an iterative, inverse approach, the age of ice at given depth  $z_i$  was derived, assuming (i) that deviations between measurements and steady-state model output as seen in Fig.1 are in first order explained by changes in past net accumulation rates and (ii) a record of it is reflected in the present-day horizontal flow velocities. Notably, the so derived, inverse modeled age-depth relationship closely aligns the empirical dating of the core (Fig. 2) and can even serve for validation. These findings indicate a great potential of displacement measurements for improved age-scale modeling and understanding of ice-flow dynamics.

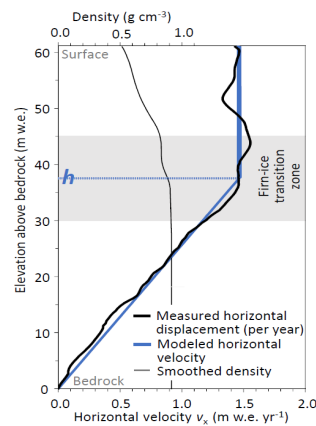


**Fig. 1** See text & legend.

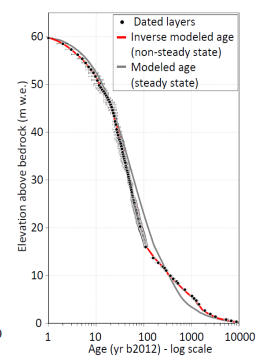


**Fig. 2** See text & legend.

- [1] C. Licciulli et al., *J. Glaciol.*, **66**, 35–48 (2020).
- [2] T. M. Jenk et al., *JGR*, **114**, D14305 (2009).
- [3] D. Buiron et al., *Clim. Past*, **7**(1), 1–16 (2011).
- [4] P. Gabrielli et al., *TC*, **10**, 2779–2797 (2016).
- [5] W. Dansgaard and S. Johnsen, *J. Glaciol.*, **8**(53), 215–223 (1969).

## PRELIMINARY RESULTS FROM THE ADAMELLO TEMPERATE ICE CORE

G. Baccolo, S. Brütsch, A. Eichler (PSI LUC), S. O. Brügger (Univ. Basel),  
M. Schwikowski (PSI LUC, Univ. Bern), P. Bohleber (Univ. Venice)

**First results from the Adamello ice core show that glaciochemical signals in temperate ice are subject to strong post-depositional effects, posing issues for paleo-climatic reconstructions.**

The Adamello glacier in the Rhaetian Alps is the largest one in Italy. Due to its low elevation (2500 to 3400 meters a.s.l.) and lack of orographic shielding, it is declining even at its highest elevations. The glacier's thermal regime is temperate: ice is in equilibrium with the liquid phase. Radar surveys showed ice thicknesses exceeding 250 m at the Pian di Neve plateau, in the high part of the glacier (~3100 m a.s.l.), with limited horizontal flow. Because of such features, in 2016 a shallow core was drilled there, revealing that the glacier preserves signals related to insoluble species and particulate matter [1]. The site is therefore ideal to explore the preservation of climatic signals in temperate ice, where meltwater is known for disturbing the original stratigraphy.

Following the success of the exploratory drilling [1], in April 2021, a 223-meter-long ice core was drilled down to bedrock in collaboration with the University of Milano-Bicocca. The ice is being analyzed at PSI for ions, trace elements, black carbon, and  $^{14}\text{C}$  for dating.

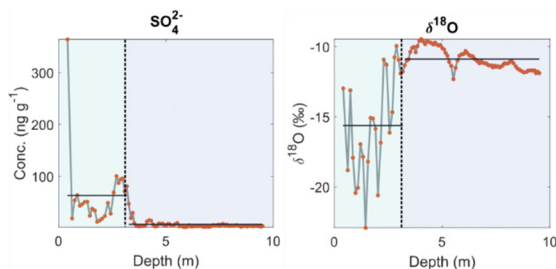


**Fig. 1:** Sulphate and stable oxygen isotopes in the upper 10 m of the Adamello ice core. The vertical dashed line marks the transition between fresh snow and ice.

So far, the upper 10 m of the ice core have been analyzed, along with deep sections to assess whether the ice composition is uniform over depth. In Fig.1, sulphate (example of ionic species) and stable oxygen isotopes ( $\delta^{18}\text{O}$ ) records are displayed. During drilling, the ice surface of the glacier was covered by winter snow, allowing exploring differences between fresh unaltered snow and temperate ice. The discontinuity, marked in Fig.1 by vertical dashed lines, is evident in the two records as an abrupt change point. The concentration of sulphate is higher in snow than in ice, where it reaches among the minimum values ever reported for Alpine ice cores. Moreover,  $\delta^{18}\text{O}$  is heavier in the ice, revealing ongoing post-depositional processes. Both the removal of ions and the enrichment in heavy isotopes have been related to meltwater percolation and runoff [2-3].

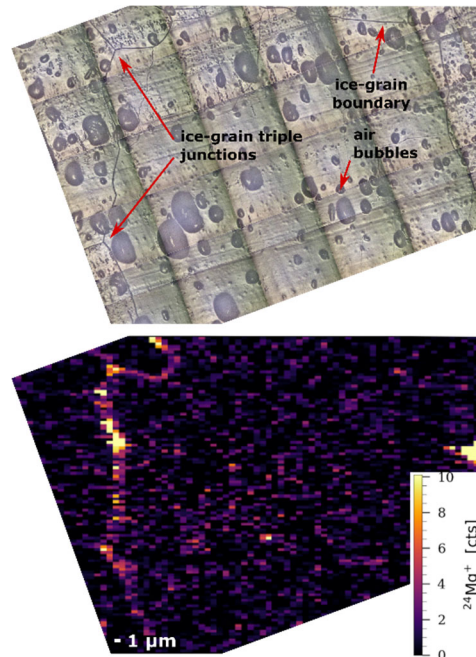


**Fig. 2:** Top: Micro-photography of ice from the Adamello ice core (134 m deep). Bottom: Same area investigated with laser ablation ICP-MS to map the distribution of trace elements in ice (Mg in this case).

To study the spatial distribution of impurities, selected samples were analysed with laser ablation ICP-MS at the University of Venice. The technique enables the distribution of trace elements in the ice to be mapped [4]. As can be seen in Fig.2, the ice is almost pure water ice, with rare impurities at grain boundaries. This confirms the predicted ability of temperate ice to self-purify itself [5]. During ice re-crystallization, impurities are expelled towards the grain junctions and washed away in the liquid vein network that is present in temperate ice.

To better comprehend the geochemical behaviour of temperate ice and its potential as a paleoclimatic archive, additional analyses will be carried out in the next months on the Adamello ice core, including trace element analyses and the application of radiocarbon for dating the ice. This will be important to assess whether in a warming Earth, it will be still possible to retrieve paleoclimatic records from glaciers that are rapidly turning to a temperate regime.

- 
- [1] D. Festi et al., *TC*, **15**, 4135-4143 (2021).
  - [2] A. Eichler et al., *Tellus B*, **53**, 192-203, (2001).
  - [3] J. Grabczak et al., *J. Glac.*, **29**, 417-424, (1983).
  - [4] P. Bohleber et al., *JAAS*, **35**, 2204-2212 (2020).
  - [5] J. W. Glen et al., in *Isotopes and impurities in snow and ice*, 263-271 (1977).

## RADIOCARBON DATING OF A SVALBARD HORIZONTAL ICE CORE

W. F. Hartz (Univ. Oxford, UNIS, NILU), T. M. Jenk (PSI LUC), T. Singer, M. Schwikowski (PSI LUC, Univ. Bern), A. Hodson (UNIS, HVL)

**A ‘horizontal ice core’ from the Foxfonna Ice Cap (FIC), Svalbard (Norwegian Arctic), demonstrates the successful  $^{14}\text{C}$  dating of dissolved (DOC) and water insoluble organic carbon (WIOC) in polar ice. First results allow conclusions about the glacial history of the Foxfonna ice cap with the site showing great potential for easy access to large volume samples for future paleoclimate studies.**

Existing ice core records from Svalbard have been limited to the past 300 years (Holtedahlfonna) to 1200 years (Lomonosovfonna) [1,2]. Numerous paleoclimate investigations on Svalbard thus relied on lacustrine and marine sediment core records to reconstruct Svalbard’s Holocene glacial history [3]. Two recent studies have undertaken  $^{14}\text{C}$  dating of subglacially preserved vegetation to constrain the timing of ice margin advances on Svalbard [4,5]. Thereby, preserved mosses with an age of 490 to 3980 years indicated the potential to find older ice preserved in cold-based glaciers on Svalbard [5].

The Foxfonna Ice Cap, located in the High Arctic archipelago of Svalbard ( $74^\circ$  to  $81^\circ\text{N}$ ), is one such cold-based glacier under which vegetation has been preserved (unpublished). It forms a cupula (1.5-1.8 km diameter) with an ice thickness of  $\sim 70$  m at the center. Recent years of negative mass balance have revealed isochrones with concentric circles (Figure 1). Unlike many existing glaciers previously studied on Svalbard, the FIC is a small, cold-based system with little glacier flow and largely wind driven accumulation with a summit elevation of  $\sim 809$  m a.s.l.. In May 2021, a horizontal ice core was retrieved by sampling at six sites along a horizontal transect from the center downslope and perpendicular to the isochrones ( $78^\circ 07.60'\text{N} / 16^\circ 10.30'\text{E}$  to  $78^\circ 07.38'\text{N} / 16^\circ 08.95'\text{E}$ ; Figure 1). At each site, 2.5 kg of ice from 1 m depth (below the seasonal snowpack and ablation surface ice) was retrieved for radiocarbon dating using DOC and WIOC, the organic fractions of the ice incorporated carbonaceous aerosol [6].

Concentration levels of DOC ranged from  $35\text{--}100 \mu\text{gC kg}^{-1}$  and from  $20\text{--}110 \mu\text{gC kg}^{-1}$  for WIOC, sufficient for  $^{14}\text{C}$  dating with around 270 g and 850 g of ice available for the respective fractions after decontamination. The DOC/WIOC ratios (0.9-2.1) were typically lower than those of preindustrial ice in the European Alps (1.5-8.0). Meltwater percolation is commonly observed on Svalbard glaciers. Since DOC will be mobilized with the meltwater, low DOC/WIOC ratios are likely a result of the loss/runoff of DOC during summer melt. Radiocarbon dates of DOC ranged from 390-1800 a cal BP and 680-1970 a cal BP for WIOC (Figure 1).

For two samples, DOC ages were significantly younger

by  $\sim 1000$  years. This cannot be explained by in-situ formation of  $^{14}\text{C}$  in DOC from cosmogenic radiation [6], with calculations estimating the potential effect to be negligible ( $< 100$  a). For WIOC, a shift towards older ages for some samples, caused by the black mineral dust visible on the filters, cannot be excluded in view of the nearby sources from natural coal shale formations (fossil,  $^{14}\text{C}$  extinct). In any case, consistent for both fractions, the oldest samples were found in the lowermost transects with ages of  $1800\pm 400$  a cal BP,  $1580\pm 370$  a cal BP (DOC) and  $1970\pm 300$  a cal BP (WIOC), suggesting neoglaciation of the FIC at least 2000 years before present. This is in line with results from a study on Longyearbreen glacier (16 km away) where subglacial vegetation was dated with 1930-1130 a cal BP [7].

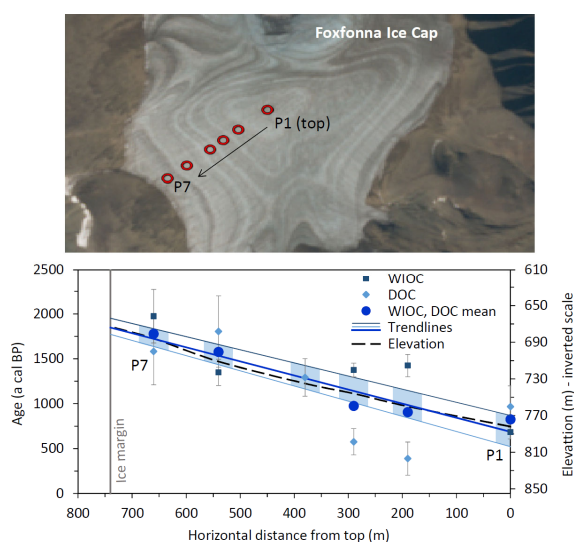


**Fig. 1** Top: Foxfonna ice cap with sampling sites. Bottom: Derived radiocarbon ages along the horizontal profile with highest age probabilities (blue shading).

We acknowledge funding by the Research Council Norway: BIOICE, Project Number 288402.

- [1] E. Beaudon et al., *J. Glaciol.*, **59**, 1069–1083 (2013).
- [2] D. Divine et al., *Polar Res.*, **30** (2011).
- [3] W. R. Farnsworth et al., *Earth-Science Rev.*, **208**, 103249 (2020).
- [4] G. H. Miller et al., *Quat. Sci. Rev.*, **155**, 67–78 (2017).
- [5] A. Roche, PhD thesis, Univ. of Norway (2021).
- [6] L. Fang et al., *The Cryosphere*, **15**, 1537–1550, (2021).
- [7] O. Humlum et al., *The Holocene*, **15**, 396–407 (2005).

## RECENT AIR POLLUTION DECREASE IN THE EURASIAN ARCTIC

R. Kron (PSI LUC, Univ. Bern), A. Eichler, S. Brüttsch (PSI LUC), T. S. Münster (PSI LUC, Univ. Bern), T. Tessendorf, T. Opel, H. Meyer (AWI), M. Schwikowski (PSI LUC, Univ. Bern)

### Shallow ice cores demonstrate that ice caps in the Russian Arctic are, despite increased temperatures, still valuable natural archives showing a significant decrease of air pollution since the 1990s.

The Arctic region is strongly affected by global warming and the recent rise in temperature is much more pronounced in this region in comparison to the global average. However, instrumental observations are scarce. Thus, ice cores come into play to document recent changes. Previous ice core studies were undertaken in the 1990s at the Akademii Nauk Ice Cap (AN) in Severnaya Zemlya [1-3] and at the Windy Dome Ice Cap (WD) in Franz Josef Land [4]. During the Arctic Century Expedition conducted in 2021, two shallow ice cores were collected at each of these two sites and one core was collected at a new site, the University (UN) Ice Cap in Severnaya Zemlya (Fig. 1). The shallow ice cores should close or shorten the window of time without data that has passed since the last drilling. They should reveal to what extent the temperature increase has generally affected the ice archives and if possible how much anthropogenic pollution has changed since the 1990s.

The five shallow ice cores had a length of 2.5 m to 7.5 m and were analyzed using a variety of methods. The ratios of stable water isotopes ( $\delta^{18}\text{O}$ ,  $\delta^2\text{H}$ ) were determined with wavelength-scanned cavity ring down spectrometry, major ions with ion chromatography, trace elements with inductively-coupled plasma sector field mass spectrometry and black carbon with single particle photometry.

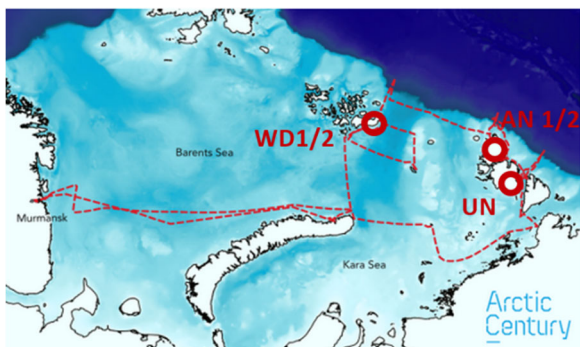


**Fig. 1:** Map of the Barents and Kara seas with the route of the Arctic Century expedition from 05.08.2021 to 06.09.2021 and the locations of the shallow core drilling sites Akademii Nauk Ice Cap (AN), Windy Dome Ice Cap (WD), and University Ice Cap (UN).

Ice-core dating based on the seasonal signals of  $\delta^{18}\text{O}$  and major ion concentrations revealed that the cores cover the periods AD 2017-2021 (AN+UN) and 2014-2021 (WD). In general, there is a considerable similarity between the respective parallel shallow cores for the majority of the investigated species, as illustrated in Fig. 2 for the AN cores. Concentrations of sea salt tracers are comparable to those of previous studies for the AN and WD sites. Since these tracers are especially prone to be removed with meltwater, there is thus no clear indication of enhanced melting in recent times. Presumably, temperatures in winter are still low enough to prevent deeper percolation of meltwater formed in summer. Consequently, the decrease in concentrations of anthropogenic tracers ( $\text{SO}_4^{2-}$ ,  $\text{NO}_3^-$ , Pb) can be interpreted as real atmospheric signal, demonstrating the effectiveness of air pollution control measures. The stable isotope ratio  $\delta^{18}\text{O}$  increased in comparison to the previous studies at AN and WD, in line with the rise in temperature. In conclusion, ice cores from the Russian Arctic still contain reliable climate and environmental information despite strong warming in recent decades.

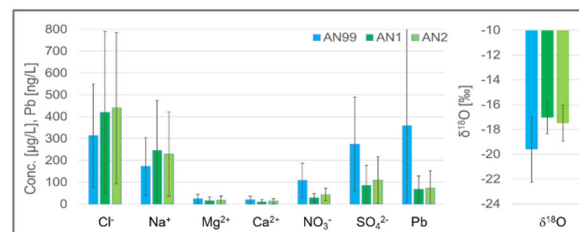


**Fig. 2:** Mean values of concentrations of major ions and Pb as well as  $\delta^{18}\text{O}$  from the previous AN99 core (1985-1999, [1-3], blue) and the cores AN1 (dark green) and AN2 (light green).

We acknowledge access to these precious ice core samples, which was possible thanks to the Arctic Century Expedition, organized jointly by the Swiss Polar Institute (SPI), the Arctic and Antarctic Research Institute (AARI) in Russia, and the Helmholtz Centre for Ocean Research Kiel (GEOMAR) in Germany.

- [1] K. Weiler et al., *J. Glac.*, **51**, 64-74 (2005).
- [2] J. R. McConnell et al., *PNAS*, **116**, 14910-14915 (2019).
- [3] T. Opel et al., *J. Glac.*, **55**, 21-31 (2009).
- [4] D. Henderson, PhD Thesis, University of Ohio (2002).

## ICE CORE ACTIVITIES IN THE PAMIR PROJECT

*M. Schwikowski (PSI LUC, Univ. Bern), T. M. Jenk, F. Burgay (PSI LUC), C. Mayer, A. Lambrecht (BAW), E. Miles (WSL)*

**Within the frame of the PAMIR project, a reconnaissance expedition was conducted to determine the optimal location for a deep ice core drilling campaign. Unfortunately, this aim was not achieved due to the unavailability of a helicopter.**

The Pamir Mountains supply water to an arid region in Central Asia stretching as far as to the Aral Sea, and buffer seasonal water shortage with snow, glacier and permafrost melt and thaw. However, the state and response of the Pamir cryosphere to climate change remains poorly understood due to a lack of measurements in the past decades. The Flagship Programme PAMIR (From ice to microorganisms and humans: Toward an interdisciplinary understanding of climate change impacts on the Third Pole) of the Swiss Polar Institute is an interdisciplinary undertaking to characterize the current state of the Pamir cryosphere to an unprecedented degree, as well as its impacts on ecosystems, hazards and water resources. One of the six programme clusters aims at extracting an ice core from the upper accumulation area of Fedchenko glacier in Tajikistan.

The Fedchenko glacier is located in the Western part of the Pamir Mountains and is with 70 km one of the longest glaciers outside Polar Regions (Fig. 1). Its potential as natural archive was recognized early on and a first shallow core was extracted in 2005, in the frame of the Central Asian Deep Ice-Coring Project [1]. That study showed that environmental signals are well preserved in the firn of the uppermost accumulation area of this glacier (above 5200 m a.s.l.). However, later attempts to collect a deep ice core have not been successful, mainly due to the remoteness of the site and the related demands for logistics. Recent accumulation and ice thickness measurements of the upper accumulation basin suggest a promising ice core drilling location near Jasgulem Pass, where the modern accumulation rate is on the order of 2 m w.e. a<sup>-1</sup> and the ice thickness reaches ~470 m [2]. With a simple glacier flow model it was estimated that an ice core from that site would cover the last millennium with annual layer thicknesses of the order of 5-10 cm. Much older ice can be expected from the lower 10% of the ice column reaching possibly back to the early Holocene [2].

We conducted a reconnaissance expedition in June/July 2022 with the aim to collect one or two shallow (10 m) firn cores, perform a radar survey to determine ice thickness, and snow pit studies for accumulation in the Jasgulem Pass. Obtained data should allow to assess the recent degree of meltwater formation at 5200 m a.s.l. and to determine the optimal location for deep drilling. The ice thickness should not exceed 200 m to allow for dry hole drilling and for reaching bedrock. An accumulation rate between 1 and 2 m w.e. a<sup>-1</sup> would be optimal,

to cover at least the last millennium with the core. Another aim of the expedition was to test the logistics for ice coring operations and ice core transport, thereby strengthening collaboration with our local partners. Unfortunately, it turned out that available helicopters and pilot qualifications were not suitable and of sufficient standard for the envisaged operation. The team abandoned the expedition without even getting close to Fedchenko glacier. Nevertheless, it was useful to strengthen the synergies between the involved partners as well as to understand "in the field", which were the main logistic difficulties and how to overcome them in view of future attempts.

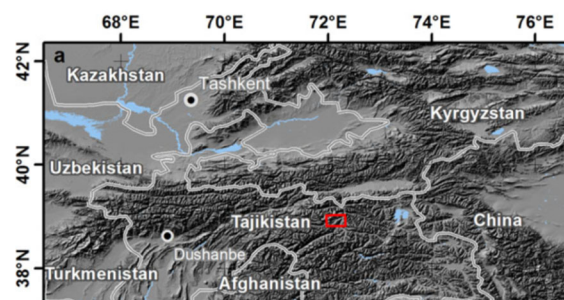


**Fig. 1:** The location of Fedchenko glacier in Central Asia (adapted from [2]).

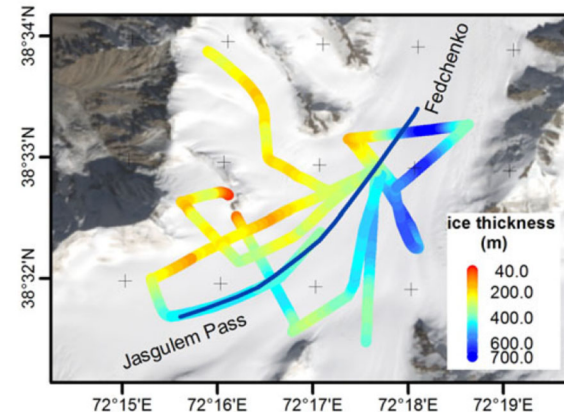


**Fig. 2:** Color-coded ice thickness along the ground-penetrating radar profiles. The background image is based on a Landsat 8 scene from 2013 (adapted from [2]).

We acknowledge funding from the Swiss Polar Institute (SPI).

- [1] V. B. Aizen et al., *J. Glac.*, **55** (190), 275-291, (2009).
- [2] A. Lambrecht et al., *J. Glac.*, **66** (256), 219-230, (2020).

## ICE CORE SCIENCES AT THE THREE POLES

*M. Schwikowski (PSI LUC, Univ. Bern), H. Fischer (KUP/Univ. Bern)*

**From 2 to 7 October 2022, the international ice core science community assembled for its third Open Science Conference (OSC) in Crans-Montana, Switzerland. The day before the OSC started, the Ice Core Young Scientist (ICYS) met for their second workshop.**

Ice cores provide information about past climate and environmental conditions as well as direct records of the composition of the atmosphere on timescales from decades to hundreds of millennia. With the pioneering work of Hans Oeschger of University of Bern on carbon dioxide in polar ice cores, a long tradition of ice core research in Switzerland began. Less known is that Hans Oeschger also initiated a high-alpine drilling project on Colle Gnifetti in Switzerland in the 1970s. To acknowledge Hans Oeschger's important contribution to these two ice core fields and to foster the link between the corresponding communities the theme of the third OSC was **Ice Core Science at the three Poles**.

The conference had been initially planned for 2020, but had to be postponed twice due to the COVID-19 pandemic. Finally, in fall 2022 the international ice core science community assembled for its third OSC in Crans-Montana, a ski resort above the Rhone Valley in Switzerland, only about 50 km from the Colle Gnifetti. The OSC brought together ice core scientists from 20 countries working on the Greenland and Antarctic Ice Sheet as well as high-altitude glaciers. Also, a few intrepid specialists from other paleoclimate science areas attended the conference. With 290 registrations (20 of them virtual) from 20 nations for the IPICS OSC and 130 participants of the ICYS workshop, this was the largest IPICS conference and the largest ICYS young scientist meeting ever.

With three poster sessions, 13 invited keynote lectures and 49 other oral presentations the scientific program of the OSC was intense and exciting, showing the creativity and scientific rigor especially of the early career scientists present, which represent the future of ice core sciences. Latest proxy developments in ice core science and from other areas of paleoclimate research, new ice

core drilling techniques, new high-resolution ice core records, and reports from and plans for new ice core projects (ranging from rescuing high-altitude glacier archives to securing the oldest ice on Earth) were presented. Moreover, the OSC was preceded by the traditional young scientist meeting organized by the ice-core early-career network organization ICYS and attended by more than 130 early-career scientists. This meeting offered insights into additional aspects of research today and instructed the attendees in various facets of science communication and research career development.

We welcomed the participants to a jolly icebreaker party, organized conference excursions to the Great Aletsch Glacier and the old town of Sion, a breath-taking theatre performance "fleeting ice - news of tomorrow" (<http://www.fluechtigeseis.ch>), a beautiful and rustic conference dinner a la Suisse, a get-together dinner for the young scientists and finished the conference off by a 1-day post-conference excursion.

However, all those plans could not be realized without the generous financial support of our sponsors and we are deeply indebted to them (<https://indico.psi.ch/event/6697/>). Apart from the many events, this generous sponsoring allowed us not only to invite 13 international keynote speakers, but - most importantly - to award 48 (!) travel grants to early career scientists from all over the world. Only this support allowed many of them to participate in the OSC and the young scientist meeting despite the large costs to travel to Switzerland. An investment into the future that hopefully will have an impact on their scientific career.

Given the success of the conference and the outstanding contributions by many early-career scientists, ice core science itself seems not at risk, and will look forward to the next IPICS OSC to be held in 2026.

---

We would like to thank all members of the local organizing committee: D. Bühler, A. Eichler, T. M. Jenk, C. Huber, T. Stocker, S. Dini and V. Hiroz.



## LIST OF PUBLICATIONS

## SURFACE CHEMISTRY

- P. A. Alpert, A. Boucly, S. Yang, H. Yang, K. Kilchhofer, Z. Luo, C. Padeste, S. Finizio, M. Ammann, B. Watts  
*Ice nucleation imaged with X-ray spectro-microscopy*  
Environmental Science: Atmospheres. 2022; **2**(3): 335-351. <https://doi.org/10.1039/D1EA00077B>
- P. A. Alpert, W. P. Kalthau, R. E. O'Brien, R. C. Moffet, M. K. Gilles, B. Wang, A. Laskin, J. Y. Aller, D. A. Knopf  
*Ice-nucleating agents in sea spray aerosol identified and quantified with a holistic multimodal freezing model*  
Science Advances. 2022; **8**(44): eabq6842 (11 pp.). <https://doi.org/10.1126/sciadv.abq6842>
- M. Ammann, L. Artiglia  
*Solvation, surface propensity, and chemical reactions of solutes at atmospheric liquid-vapor interfaces*  
Accounts of Chemical Research. 2022; **55**(24): 3641-3651. <https://doi.org/10.1021/acs.accounts.2c00604>
- V. J. Baboomian, G. V. Crescenzo, Y. Huang, F. Mahrt, M. Shiraiwa, A. K. Bertram, S. A. Nizkorodov  
*Sunlight can convert atmospheric aerosols into a glassy solid state and modify their environmental impacts*  
Proceedings of the National Academy of Sciences of the United States of America PNAS. 2022; **119**(43): e2208121119 (10 pp.). <https://doi.org/10.1073/pnas.2208121119>
- A. Boucly, L. Artiglia, E. Fabbri, D. Palagin, D. Aegerter, D. Pergolesi, Z. Novotny, N. Comini, J. T. Diulus, T. Huthwelker, M. Ammann, T. J. Schmidt  
*Direct evidence of cobalt oxyhydroxide formation on a La<sub>0.2</sub>Sr<sub>0.8</sub>CoO<sub>3</sub> perovskite water splitting catalyst*  
Journal of Materials Chemistry A. 2022; **10**(5): 2434-2444. <https://doi.org/10.1039/D1TA04957G>
- P. Corral Arroyo, G. David, P. A. Alpert, E. A. Parmentier, M. Ammann, R. Signorell  
*Amplification of light within aerosol particles accelerates in-particle photochemistry*  
Science. 2022; **376**(6590): 293-296. <https://doi.org/10.1126/science.abm7915>
- I. Gladich, S. Chen, H. Yang, A. Boucly, B. Winter, J. A. van Bokhoven, M. Ammann, L. Artiglia  
*Liquid-gas interface of iron aqueous solutions and Fenton reagents*  
Journal of Physical Chemistry Letters. 2022; **13**(13): 2994-3001. <https://doi.org/10.1021/acs.jpcllett.2c00380>
- I. Gladich, S. Chen, H. Yang, A. Boucly, B. Winter, J. A. van Bokhoven, M. Ammann, L. Artiglia  
*Reply to "comment on 'liquid-gas interface of iron aqueous solutions and fenton reagents'"*  
Journal of Physical Chemistry Letters. 2022; **13**(29): 6681-6682. <https://doi.org/10.1021/acs.jpcllett.2c01391>
- X. Kong, J. Dou, S. Chen, B. Wang, Z. Wu  
同步辐射技术在大气科学领域的研究进展. *Progress of synchrotron-based research on atmospheric science*  
Progress in Chemistry. 2022; **34**(4): 963-972. <https://doi.org/10.7536/PC210438>
- K. D. Kulju, S. M. McNamara, Q. Chen, H. S. Kenagy, J. Edebeli, J. D. Fuentes, S. B. Bertman, K. A. Pratt  
*Urban inland wintertime N<sub>2</sub>O<sub>5</sub> and ClNO<sub>2</sub> influenced by snow-covered ground, air turbulence, and precipitation*  
Atmospheric Chemistry and Physics. 2022; **22**(4): 2553-2568. <https://doi.org/10.5194/acp-22-2553-2022>
- F. Mahrt, L. Peng, J. Zaks, Y. Huang, P. E. Ohno, N. R. Smith, F. K. A. Gregson, Y. Qin, C. L. Faiola, S. T. Martin, S. A. Nizkorodov, M. Ammann, A. K. Bertram  
*Not all types of secondary organic aerosol mix: two phases observed when mixing different secondary organic aerosol types*  
Atmospheric Chemistry and Physics. 2022; **22**(20): 13783-13796. <https://doi.org/10.5194/acp-22-13783-2022>
- F. Mahrt, Y. Huang, J. Zaks, A. Devi, L. Peng, P. E. Ohno, Y. M. Qin, S. T. Martin, M. Ammann, A. K. Bertram  
*Phase behavior of internal mixtures of hydrocarbon-like primary organic aerosol and secondary aerosol based on their differences in oxygen-to-carbon ratios*  
Environmental Science and Technology. 2022; **56**(7): 3960-3973. <https://doi.org/10.1021/acs.est.1c07691>
- P. E. Ohno, J. Wang, F. Mahrt, J. G. Varelas, E. Aruffo, J. Ye, Y. Qin, K. J. Kiland, A. K. Bertram, R. J. Thomson, S. T. Martin  
*Gas-Particle uptake and hygroscopic growth by organosulfate particles*  
ACS Earth and Space Chemistry. 2022; **6**(10): 2481-2490. <https://doi.org/10.1021/acsearthspacechem.2c00195>

Y. Uemura, A. S. M. Ismail, S. H. Park, S. Kwon, M. Kim, H. Elnaggar, F. Frati, H. Wadati, Y. Hirata, Y. Zhang, K. Yamagami, S. Yamamoto, I. Matsuda, U. Halisdemir, G. Koster, C. Milne, M. Ammann, B. M. Weckhuysen, F. M. F. de Groot

*Hole dynamics in photoexcited hematite studied with femtosecond oxygen K-edge X-ray absorption spectroscopy*  
Journal of Physical Chemistry Letters. 2022; **13**(19): 4207-4214. <https://doi.org/10.1021/acs.jpcllett.2c00295>

S. Xu, F. Mahrt, F. K. A. Gregson, A. K. Bertram

*Possible effects of ozone chemistry on the phase behavior of skin oil and cooking oil films and particles indoors*  
ACS Earth and Space Chemistry. 2022; **6**(7): 1836-1845. <https://doi.org/10.1021/acsearthspacechem.2c00092>

H. Yang, I. Gladich, A. Boucly, L. Artiglia, M. Ammann

*Orcinol and resorcinol induce local ordering of water molecules near the liquid-vapor interface*  
Environmental Science: Atmospheres. 2022; **2**(6): 1239-1570. <https://doi.org/10.1039/d2ea00015f>

## ANALYTICAL CHEMISTRY

F. Aemisegger, J. Trachsel, Y. Sadowski, A. Eichler, M. Lehning, S. Avak, M. Schneebeli

*Fingerprints of frontal passages and post-depositional effects in the stable water isotope signal of seasonal Alpine snow*  
Journal of Geophysical Research D: Atmospheres. 2022; **127**(22): e2022JD037469 (20 pp.). <https://doi.org/10.1029/2022JD037469>

M. Barandun, C. Bravo, B. Grobety, T. M. Jenk, L. Fang, K. Naegeli, A. Rivera, S. Cisternas, T. S. Münster, M. Schwikowski

*Anthropogenic influence on surface changes at the Olivares glaciers; Central Chile*  
Science of the Total Environment. 2022; **833**: 155068 (18 pp.). <https://doi.org/10.1016/j.scitotenv.2022.155068>

A. Beschnitt, M. Schwikowski, T. Hoffmann

*Towards comprehensive non-target screening using heart-cut two-dimensional liquid chromatography for the analysis of organic atmospheric tracers in ice cores*  
Journal of Chromatography A. 2022; **1661**: 462706 (12 pp.). <https://doi.org/10.1016/j.chroma.2021.462706>

H. M. Clifford, M. Potocki, C. Rodda, D. Dixon, S. Birkel, M. Handley, E. Korotkikh, D. Introne, F. Schwanck, F. A. Tavares

*Prefacing unexplored archives from Central Andean surface-to-bedrock ice cores through a multifaceted investigation of regional firn and ice core glaciochemistry*  
Journal of Glaciology. 2022: 1-15. <https://doi.org/10.1017/jog.2022.91>

K. O. Moseid, M. Schulz, A. Eichler, M. Schwikowski, J. R. McConnell, D. Olivié, A. S. Criscitello, K. J. Kreutz, M. Legrand

*Using ice cores to evaluate CMIP6 aerosol concentrations over the historical era*  
Journal of Geophysical Research D: Atmospheres. 2022; **127**(18): e2021JD036105 (21 pp.). <https://doi.org/10.1029/2021JD036105>

M. Potocki, P. A. Mayewski, T. Matthews, L. B. Perry, M. Schwikowski, A. M. Tait, E. Korotkikh, H. Clifford, S. Kang, T. C. Sherpa, P. K. Singh, I. Koch, S. Birkel

*Mt. Everest's highest glacier is a sentinel for accelerating ice loss*  
npj Climate and Atmospheric Science. 2022; **5**: 7 (8 pp.). <https://doi.org/10.1038/s41612-022-00230-0>

F. Scoto, H. Sadatzki, N. Maffezzoli, C. Barbante, A. Gagliardi, C. Varin, P. Vallelonga, V. Gkinis, D. Dahl-Jensen, H. A. Kjær, F. Burgay, A. Saiz-Lopez, R. Stein, A. Spalor

*Sea ice fluctuations in the Baffin Bay and the Labrador Sea during glacial abrupt climate changes*  
Proceedings of the National Academy of Sciences of the United States of America PNAS. 2022; **119**(44): e2203468119 (9 pp.). <https://doi.org/10.1073/pnas.2203468119>

W. Zhang, S. Hou, S.-Y. Wu, H. Pang, S. B. Sneed, E. V. Korotkikh, P. A. Mayewski, T. M. Jenk, M. Schwikowski

*A quantitative method of resolving annual precipitation for the past millennia from Tibetan ice cores*  
Cryosphere. 2022; **16**(5): 1997-2008. <https://doi.org/10.5194/tc-16-1997-2022>

## AFFILIATION INDEX

AWI	Alfred-Wegener-Institut, Helmholtz-Zentrum für Polar- und Meeresforschung, Telegrafenberg A45, 14473 Potsdam, Germany
BAdW	Bayrische Akademie der Wissenschaften, Alfons-Goppel-Strasse 11, 80539 München, Germany
CUB	CU Boulder, University of Colorado, Boulder, CO 80309, USA
ENE	Department of Energy and Environment, Paul Scherrer Institut, 5232 Villigen, Switzerland
ETHZ	ETH Zürich, Eidgenössische Technische Hochschule Zürich, 8092 Zürich, Switzerland
FHI	Fritz-Haber-Institut der Max-Planck-Gesellschaft, Faradayweg 4-6, 14195 Berlin, Germany
HU	Harvard University, Center for the Environment, 28 Oxford Street, Cambridge, MA 02138, USA
HVL	Høgskulen på Vestlandet (Western Norway University of Applied Sciences), Inndalsveien 28, 5063 Bergen, Norway
INM Minsk	Institute for Nature Management, Laboratory of Transboundary Pollution, National Academy of Sciences of Belarus, Skoriny str. 10, 220076 Minsk, Belarus
IWEP	Institute for Water and Environmental Problems, Ulitsa Molodezhnaya, 1, Barnaul 656038, Altai Krai, Russia
KUP/Univ. Bern	Universität Bern, Klima und Umweltp Physik, Sidlerstrasse 5, 3012 Bern, Switzerland
LAC	Laboratory for Atmospheric Chemistry, Paul Scherrer Institut, 5232 Villigen, Switzerland
LBK	Bioenergy and Catalysis Laboratory, Paul Scherrer Institut, 5232 Villigen, Switzerland
LEC	Electro Chemistry Laboratory, Paul Scherrer Institut, 5232 Villigen, Switzerland
LMS	Laboratory for Materials Simulations, Paul Scherrer Institut, 5232 Villigen, Switzerland
LSK	Laboratory for Catalysis and Sustainable Chemistry, Paul Scherrer Institut, 5232 Villigen, Switzerland
LUC	Laboratory of Environmental Chemistry, Paul Scherrer Institut, 5232 Villigen, Switzerland
MPIC	Max-Planck-Institut für Chemie, Hahn-Meitner-Weg 1, 55128 Mainz, Germany
NILU	Climate and Environmental Research Institute, Instituttveien 18, 2007 Kjeller, Norway
NUM	Research with Neutrons and Muons, Paul Scherrer Institut, 5232 Villigen, Switzerland
PhLAM	Laboratoire de Physique des Lasers, Atomes et Molecules, Université de Lille, 2 Avenue Jean Perrin, 59655 Villeneuve d'Ascq Cedex, France
PSI	Paul Scherrer Institut, Forschungsstrasse 111, 5232 Villigen, Switzerland
UBC	The University of British Columbia, Vancouver Campus, 2329 West Mall, Vancouver V6T 1Z4, Canada
UCI	University of California Irvine, Irvine, CA 92697, USA
UCLA	University of California, Atmospheric & Oceanic Sciences, Box 951565, Los Angeles, CA 90095-1565, USA
UNIS	The University Centre in Svalbard, P. O. Box 156, 9171 Longyearbyen, Norway
UNITO	Italian Glaciological Committee, c/o Università di Torino, Via Verdi, 8, 10124 Torino, Italy
Univ. Bern	Universität Bern, Departement für Chemie, Biochemie und Pharmazie, Freiestrasse 3, 3012 Bern, Switzerland
Univ. Basel	Universität Basel, Departement Umweltwissenschaften, Klingelbergstrasse 27, 4056 Basel, Switzerland
Univ. Grenoble	Université Grenoble Alpes, Institut des Géosciences de l'Environnement, CS 40700, 38058 Grenoble Cedex 9, France
Univ. Oxford	University of Oxford, Department of Earth Sciences, South Parks Road, Oxford OX1 3AN, UK
Univ. Venice	Università Ca' Foscari Venezia, Dorsoduro 3246, 30123 Venezia, Italy
WSL	Eidg. Forschungsanstalt für Wald, Schnee und Landschaft, Zürcherstrasse 111, 8903 Birmensdorf, Switzerland

Paul Scherrer Institut :: 5232 Villigen PSI :: Switzerland :: Tel. +41 56 310 21 11 :: [www.psi.ch](http://www.psi.ch)

